

HEAVY QUARK PRODUCTION IN HADRON COLLISIONS

M.G.Ryskin, Yu.M.Shabelski and A.G.Shuvaev
Petersburg Nuclear Physics Institute,
Gatchina, St.Petersburg 188350 Russia

*Lecture, given at XXXIV PNPI Winter School,
St.Petersburg, 2000*

Abstract

We compare the numerical predictions for heavy quark production in high energy hadron collisions of the conventional QCD parton model and the k_T -factorization approach (semihard theory). The total production cross sections, one-particle rapidity and p_T distributions as well as several two-particle correlations are considered. Some of them can help to estimate QCD scale. The difference in the predictions of the two approaches is not very large, while the shapes of the distributions are slightly different.

E-mail RYSKIN@THD.PNPI.SPB.RU

E-mail SHABELSK@THD.PNPI.SPB.RU

E-mail SHUVAEV@THD.PNPI.SPB.RU

1 Introduction

The investigation of heavy quark production in high energy hadron collisions is an important method for studying the quark-gluon structure of hadrons. Realistic estimates of the cross section of heavy quark production as well as their correlations are necessary in order to plan experiments on existing and future accelerators or in cosmic ray physics.

The description of hard interactions in hadron collisions within the framework of QCD is possible only with the help of some phenomenology, which reduces the hadron-hadron interaction to the parton-parton one via the formalism of the hadron structure functions. The cross sections of hard processes in hadron-hadron interactions can be written as the convolutions squared matrix elements of the sub-process calculated within the framework of QCD, with the parton distributions in the colliding hadrons.

The most popular and technically simplest approach is the so-called QCD collinear approximation, or parton model (PM). In this model all particles involved are assumed to be on mass shell, carrying only longitudinal momenta, and the cross section is averaged over two transverse polarizations of the incident gluons. The virtualities q^2 of the initial partons are taken into account only through their structure functions. The cross sections of QCD subprocess are calculated usually in the leading order (LO), as well as in the next to leading order (NLO) [1, 2, 3, 4, 5]. The transverse momenta of the incident partons are neglected in the QCD matrix elements. This is the direct analogy of the Weizsaecker-Williams approximation in QED. It allows to describe reasonably [6] the experimental data on the total cross sections and one-particle distributions of produced heavy flavours¹, however it can not reproduce, say, the azimuthal correlations [8] of two heavy quarks and the distributions of total transverse momentum of heavy quarks pairs [6], which are determined by the transverse momenta of the incident partons.

There is an attempt to incorporate the transverse momenta of the incident partons by a random shift of these momenta (k_T kick) [6] according to certain exponential distributions. This allows to describe quantitatively the two-particle correlations [6], but it creates the problems in the simultaneous description of one-particle longitudinal and transverse momentum distributions [9]. At the same time this procedure has no serious theoretical background. While the shift of the order of Λ_{QCD} ($\langle k_T \rangle \sim 300$ MeV) looks to be reasonable as having an possible origin in confinement forces at large distances, the values $\langle k_T \rangle \sim 1$ GeV [6], or even 3-4 GeV [10, 11] should be explained in terms of the perturbative QCD.

Another possibility to incorporate the incident parton transverse momenta is referred to as k_T -factorization approach [12, 13, 14, 15, 16, 17], or the theory of semihard interactions [18, 19, 20, 21, 22, 23, 24]. Here the Feynman diagrams are calculated taking account of the virtualities and of all possible polarizations of the incident partons. In the small x domain there are no grounds to neglect the transverse momenta of the gluons, q_{1T} and q_{2T} , in comparison with the quark mass and transverse momenta, p_{iT} . Moreover, at very high energies and very high p_{iT} the main contribution to the cross

¹New FNAL data [7] on beauty production are 2-3 times higher than the NLO parton model predictions.

sections comes from the region of $q_{1T} \sim p_{1T}$ or $q_{2T} \sim p_{1T}$, see Sect. 4 for details. The QCD matrix elements of the sub-processes are rather complicated in such an approach. We have calculated them in the LO. On the other hand, the multiple emission of soft gluons is included here. That is why the question arises as to which approach is more constructive.

The predictions of all phenomenological approaches rely on the quark and gluon structure functions. The last ones are more or less known experimentally from the data of HERA, but unknown at very small values of Bjorken variable $x < 10^{-4}$. However it is just the region that dominates in the heavy quark production at high energies². A more serious problem is probably related to the fact that the NLO parton model formalism is based on the conventional structure functions whereas the k_T -factorization approach uses so-called unintegrated distributions which, at the moment, are known with the accuracy not good enough.

In Sect. 2 we shortly discuss the conventional NLO parton model and show some numerical results together with the experimental data. The main formalism of the k_T -factorization approach is presented in Sect. 3.

In Sect. 4 we present a comparison of results [28] obtained with the help of k_T -factorization and the parton model. The main goal of this Section is to demonstrate the differences in the qualitative predictions coming from the matrix elements. To simplify the calculations and to avoid various additional dependences we have used a "toy" gluon distribution which has only a reasonable qualitative behaviour and a fixed value of α_S .

More accurate comparison [29] between the conventional parton model results and the k_T -factorization approach is given in Sect. 5 for the experimentally measured quantities. Here we have used more realistic gluon distribution GRV94 [30] which is compatible with the most recent data, see discussion in Ref. [31]. Predictions of the k_T -factorization approach for several heavy quark correlations (some of them have never been discussed before) are presented in Sect. 6.

2 Conventional parton model approach

The conventional parton model expression for the calculation of heavy quark hadroproduction cross sections has the factorized form [32]:

$$\sigma(ab \rightarrow Q\bar{Q}) = \sum_{ij} \int dx_i dx_j G_{a/i}(x_i, \mu_F) G_{b/j}(x_j, \mu_F) \hat{\sigma}(ij \rightarrow Q\bar{Q}) , \quad (1)$$

where $G_{a/i}(x_i, \mu_F)$ and $G_{b/j}(x_j, \mu_F)$ are the structure functions of partons i and j in the colliding hadrons a and b , μ_F is the factorization scale (i.e. the value of the order of the maximal virtuality of incident partons) and $\hat{\sigma}(ij \rightarrow Q\bar{Q})$ is the cross section of

²For example, in the case of charm production, $m_c = 1.4\text{GeV}$, at LHC, $\sqrt{s} = 14\text{ TeV}$, the product $x_1 x_2$ of two gluons (both x_1 and x_2 are the integral variables) is equal to $4 \cdot 10^{-8}$ and applicability of the existing structure functions seems not to be clear at so small x , see discussion in [25]. Another problem at very small x can be connected to gluon shadowing [19, 22, 26, 27]

the subprocess which is calculated in perturbative QCD. The latter cross section can be written as a sum of LO and NLO contributions,

$$\hat{\sigma}(ij \rightarrow Q\bar{Q}) = \frac{\alpha_s^2(\mu_R)}{m_Q^2} \left(f_{ij}^{(o)}(\rho) + 4\pi\alpha_s(\mu_R) [f_{ij}^{(1)}(\rho) + \bar{f}_{ij}^{(1)}(\rho) \ln(\mu^2/m_Q^2)] \right), \quad (2)$$

where μ_R is the renormalization scale and $f_{ij}^{(o)}$ as well as $f_{ij}^{(1)}$ and $\bar{f}_{ij}^{(1)}$ depend only on the single variable

$$\rho = \frac{4m_Q^2}{\hat{s}}, \quad \hat{s} = x_i x_j s_{ab}. \quad (3)$$

(In the factor $\ln(\mu^2/m_Q^2)$ we assume $\mu_R = \mu_F$ following [1]. In the case of different values of μ_R and μ_F , which is preferable for the description of the experimental data [6], Eq. (2) becomes more complicated.)

The expression (1) corresponds to the process shown schematically in Fig. 1 with $q_{iT} = q_{jT} = 0$. The main contribution to the cross section at small x is known to come from gluons, $i = j = g$.

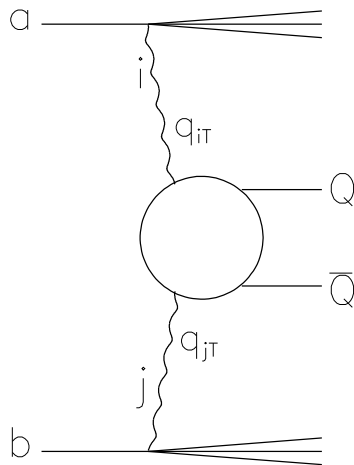


Fig. 1. Heavy quark production in hadron-hadron collision. The LO parton model corresponds to the case when $q_{1t} = q_{2t} = 0$.

The principal uncertainties of any numerical QCD calculation are the consequences of unknown scales ³, μ_F and μ_R and the heavy quark mass, m_Q . Both scales (sometimes they are assumed to be equal) are to be of the order of hardness of the treated

³These uncertainties have to disappear after all high order contributions are summed up. There is the opinion that the strong (weak) scale dependence in LO or NLO means the large (small) contribution

process, however which value is better to take, m_Q , $m_T = \sqrt{m_Q^2 + p_T^2}$ or \hat{s} , remains to be unknown. In principle, the uncertainties should not be essential because of the logarithmical dependence on these parameters. Unfortunately the masses of c and b quarks are not large enough and it leads to numerically large uncertainties (see e.g. [6]) at the existing energies for fixed target experiments.

Usually in the parton model the values

$$\mu_F = \mu_R = m_Q \quad (4)$$

are used for the total cross sections and

$$\mu_F = \mu_R = m_T = \sqrt{m_Q^2 + p_Q^2} \quad (5)$$

for the one-particle distributions [6].

Here we calculate the total cross sections of heavy quark production as the integrals over their p_T distributions, i.e. with the scales (5).

Both in the parton model and in the k_T -factorization approach we take

$$m_c = 1.4 \text{ GeV}, \quad m_b = 4.6 \text{ GeV} , \quad (6)$$

for the values of short-distance perturbative quark masses [33, 34].

Another principal problem of the parton model is the collinear approximation. The transverse momenta of the incident partons, q_{iT} and q_{jT} are assumed to be zero, and their virtualities are accounted for through the structure functions only; the cross section $\hat{\sigma}(ij \rightarrow Q\bar{Q})$ is assumed to be independent of these virtualities. Naturally, this approximation significantly simplifies the calculations.

The NLO parton model calculations of the total cross sections of $c\bar{c}$ and $b\bar{b}$ production, as functions of the beam energy, for π^-N and $p-N$ collisions can be found in [6]. These results depend strongly (by the factor of several times) on the numerical values of quark masses as well as on the both scales, μ_F and μ_R . Although there is a contradiction in some experimental data generally (at fixed target energy) they are in agreement with NLO parton model predictions.

The NLO corrections to one-particle distributions lead only to renormalization of the LO results, practically without changing in the shapes of the distributions [35, 8]. It means that instead of the more complicated NLO calculation of the p_T or rapidity distributions it is enough to calculate them in LO, and to multiply then by K-factor

$$K = \frac{LO + NLO}{LO} , \quad (7)$$

which can be taken, say, from the results on the total production cross sections. The comparison of LO + NLO calculations with the LO multiplied by the K-factor is presented in Fig. 2 taken from Ref. [35].

of high order diagrams, but it is not the case. The strong or weak scale dependence in LO or NLO indicates only the same dependence for the higher orders, which could be numerically small or large at some particular fixed scale.

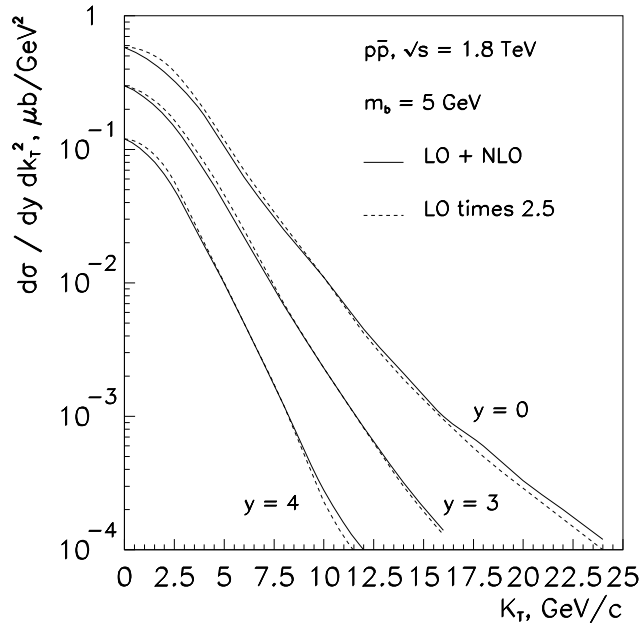


Fig. 2. The calculated p_T -distributions for $p\bar{p} \rightarrow b + X$ at $\sqrt{s} = 1.8$ TeV, for different values of rapidity for LO+NLO QCD parton model and for LO contribution multiplied by K-factor, Eq. (7) equal to 2.5.

The values of K-factors and their energy and scale dependences for the various sets of structure functions were calculated in Refs. [36, 37]. These dependences are similar for the modern sets of structure functions.

The experimental data of WA92 [38] and E769 [39] for x_F -distributions of D-mesons produced in πN interactions are in agreement with the parton model distributions for bare quarks, as one can see in Fig. 3 taken from [6]. It means that the fragmentation processes are not important here, or they are compensated by, say, recombination processes. The shape of x_F -distributions does not depend practically on the mass of c -quark.

It was claimed in [6] that the data on one-particle p_T -distributions, both obtained by fixed target experiments and by hadronic colliders (D0, CDF and UA1 collaborations) for the case of beauty production can be described by the NLO parton model using the variation of both scales, μ_R and μ_F . However new FNAL data on beauty production [7] are 2-3 times higher than the theoretical curve [8].

More serious problem appears when we consider the correlations of produced heavy quarks. Let us start from so-called azimuthal correlation. The azimuthal angle ϕ is defined as an opening angle between two produced heavy quarks, projected onto a plane perpendicular to the beam and defined as the xy -plane. In the LO parton model the sum of the produced heavy quark momenta projected onto this plane is exactly zero,

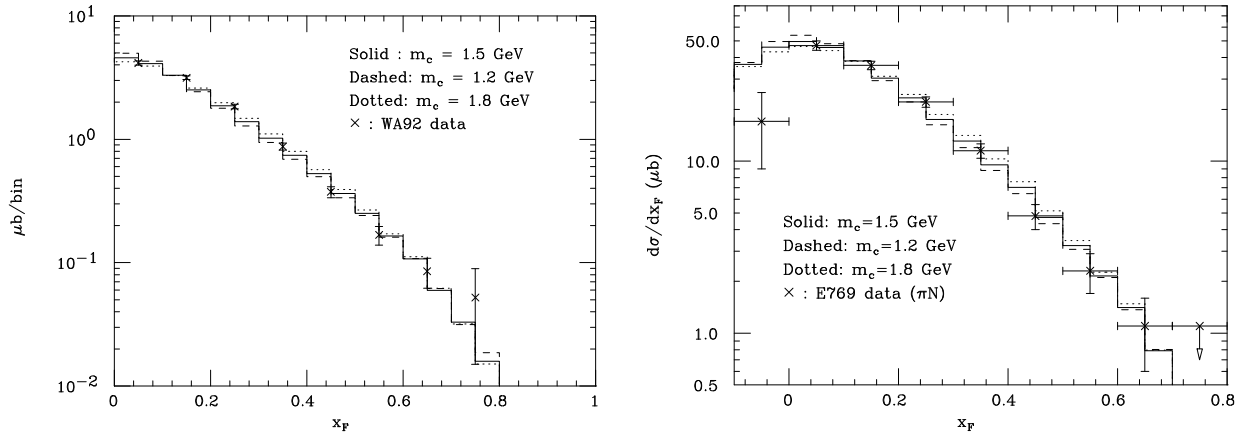


Fig. 3. Experimental x_F distributions for D mesons, compared to the NLO parton model prediction for charm quarks.

and the angle between them is always 180° . In the case of the NLO parton model the ϕ distribution is non-trivial [8], however the predicted distribution (without including the k_T kick) is narrower in comparison with the fixed target data [6].

The investigation of such distributions is very important. The relative LO and NLO contributions of the parton model depend on the unknown scales, μ_F and μ_R . In the one-particle distributions, the sum of these contributions practically coincides with the LO contribution multiplied by the K -factor, as it is shown in Fig. 2. Therefore we are unable to control separately the magnitudes of the LO and NLO contributions. Contrary, in the case of azimuthal correlations all difference from the simple $\delta(\phi - \pi)$ distribution comes from the NLO contribution.

The experimental data on azimuthal correlations are claimed (see [40, 41] and Refs. therein) to be in disagreement with the NLO predictions, for the cases of charm pair hadro- and photoproduction at fixed target energies. The level of the disagreement can be seen in Fig. 4 (solid histograms) taken from Ref. [6]. These data can be described [6], assuming the comparatively large intrinsic transverse momenta of incoming partons (k_T kick). For each event, in the longitudinal centre-of-mass frame of the heavy quark pair, the $Q\bar{Q}$ system is boosted to rest. Then a second transverse boost is performed, which gives the pair a transverse momentum equal to $\vec{p}_T(Q\bar{Q}) = \vec{k}_T(1) + \vec{k}_T(2)$; $\vec{k}_T(1)$ and $\vec{k}_T(2)$ are the transverse momenta of the incoming partons, which are chosen randomly, with their moduli distributed according to

$$\frac{1}{N} \frac{dN}{dk_T^2} = \frac{1}{\langle k_T^2 \rangle} \exp(-k_T^2 / \langle k_T^2 \rangle). \quad (8)$$

The dashed and dotted histograms in Fig. 4 correspond to the NLO parton model prediction, supplemented with the k_T kick with $\langle k_T^2 \rangle = 0.5 \text{ GeV}^2$ and $\langle k_T^2 \rangle = 1 \text{ GeV}^2$, respectively. We see that with $\langle k_T^2 \rangle = 1 \text{ GeV}^2$ it is possible [6] to describe the data.

However the large intrinsic transverse momentum significantly changes one-particle

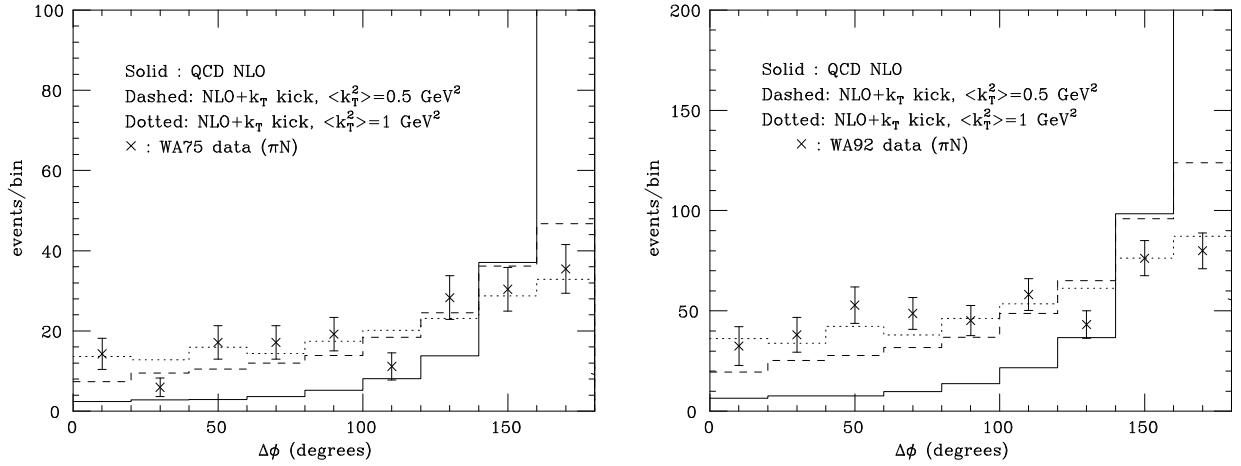


Fig. 4. Azimuthal correlation for charm production in πN collisions: NLO parton model and k_T kick calculations versus the WA75 and WA92 data.

p_T -distributions of heavy flavour hadrons, which were earlier in good agreement with the data. The solid curves in Fig. 5 taken from [6] represent the NLO parton model predictions for charm quarks p_T -distributions which are in agreement with the data. The effect of the k_T kick results in a hardening of the p_T^2 spectrum. On the other hand, by combining the k_T kick with $\langle k_T^2 \rangle = 1 \text{ GeV}^2$ and the Peterson fragmentation [42], the theoretical predictions slightly undershoot the data (dot-dashed curves). For the predictions at higher energy the values $\langle k_T^2 \rangle = 3\text{-}4 \text{ GeV}^2$ [10, 11] were used without any connection with perturbative QCD diagrams.

The k_T kick affects the x_F -distributions of the produced c -quarks very weakly, Fig. 3, and after accounting the fragmentation these distributions become too soft.

The general phenomenological expression for the heavy quark production can be written⁴ as a convolution of the initial transverse momenta distributions, $I(q_{1T})$ and $I(q_{2T})$, with squared modulo of the matrix element,

$$\sigma_{QCD}(Q\bar{Q}) \propto \int d^2 q_{1T} d^2 q_{2T} I(q_{1T}) I(q_{2T}) |M(q_{1T}, q_{2T}, p_{1T}, p_{2T})|^2. \quad (9)$$

Here there are two possibilities:

- i) the typical gluon transverse momenta are much smaller than the transverse momenta of produced heavy quarks, $q_{iT} \ll p_{iT}$, or
- ii) all transverse momenta are of the same order, $q_{iT} \sim p_{iT}$.

In the first case one can replace both initial distributions $I(q_{iT})$ by δ -functions. It reduces the expression (9) to the simple form (collinear approximation):

$$\sigma_{coll.}(Q\bar{Q}) \propto |M(0, 0, p_{1T}, p_{2T})|^2 \quad (10)$$

in total agreement with Weizsaecker-Williams approximation.

⁴We omit here for the simplicity all unimportant factors.

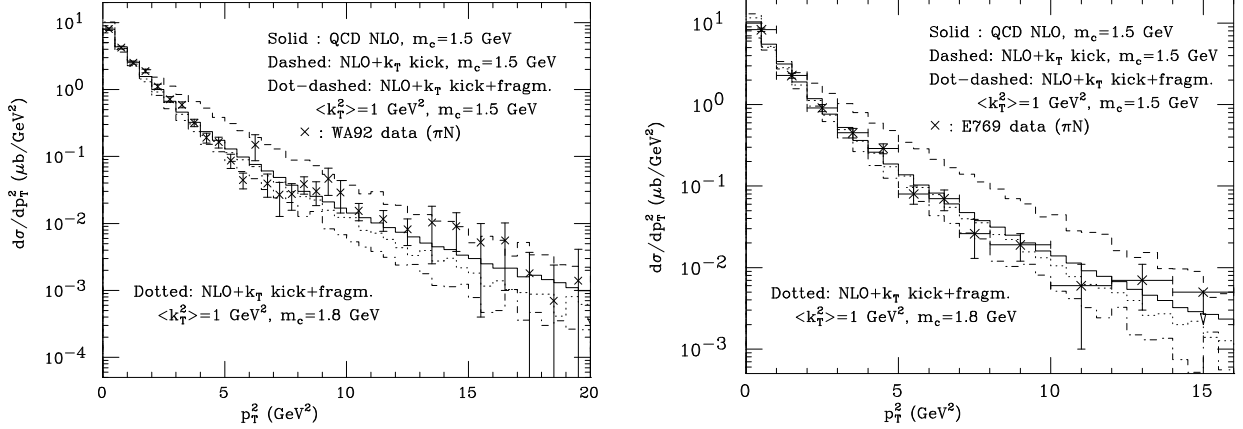


Fig. 5. Charm p_T^2 distribution measured by WA92 and E769, compared to the NLO parton model predictions, with and without the non-perturbative effects.

In the second case we can not a priori expect good results from the Weizsaecker-Williams approximation. However it gives the reasonable numerical results in some cases.

The k_T kick [6] discussed above effectively accounts for the transverse momenta of incident partons. It is based on the expression which symbolically reads

$$\sigma_{kick}(Q\bar{Q}) \propto I(q_{1T})I(q_{2T}) \otimes |M(0, 0, p_{1T}, p_{2T})|^2 \quad (11)$$

that has no good theoretical background.

The main difference from the general QCD expression, Eq. (9), is that due to the absence of q_{iT} in the matrix element the value $\langle k_T^2 \rangle$ has to be differently taken for different processes (say, for heavy flavour production with comparatively small or large p_T). The reason is that the functions $I(q_{iT})$ in general QCD expression decrease for large q_{iT}^2 as a weak power (see next Sect.), i.e. comparatively slowly, and the q_{iT}^2 dependence of the matrix element is more important.

In the last one the corrections of the order of q_{iT}^2/μ^2 , where μ^2 is the QCD scale, are small enough when $q_{iT}^2/\mu^2 \ll 1$ and they start to suppress the matrix element value when $q_{iT}^2/\mu^2 \sim 1$. Thus the essential values of the q_{iT}^2 depend on the hardness of the process.

3 Heavy quark production in the k_T -factorization approach

The transverse momenta of the incident gluons in the small- x region result in the k_T -factorization approach from $\alpha_S \ln k_T^2$ gluon diffusion. The diffusion is described by the so-called unintegrating gluon distribution - the function $\varphi(x, q^2)$ giving the gluon density

at the fixed fraction of the longitudinal momentum of the initial hadron, x , and the gluon virtuality, q^2 . These distributions should be found with the help of evolution equation and the experimental data. Unfortunately, it is not yet fulfilled. At very low x , that is to leading $\log(1/x)$ accuracy, the unintegrating gluon distribution are approximately determined [18] via the derivative of the usual structure function:

$$\varphi(x, q^2) = 4\sqrt{2}\pi^3 \frac{\partial[xG(x, q^2)]}{\partial q^2}. \quad (12)$$

Such a definition of $\varphi(x, q^2)$ enables to treat correctly the effects arising from the gluon virtualities.

Although generally φ is a function of three variables, x , q_T and q^2 , the transverse momentum dependence is comparatively weak since $q_T^2 \approx -q^2$ for small x in LLA in agreement with q^2 -dependences of structure function. Note that due to QCD scaling violation at larger q^2 , the value of $\varphi(x, q^2)$ for the realistic structure functions increases faster with decreasing of x . Therefore the larger q_T becomes important at small x in the numerical calculations.

The exact expression of the q_T gluon distribution can be obtained as a solution of the evolution equation which, contrary to the parton model case, is nonlinear due to interactions between the partons in the small x region. The calculations [43] of the q_T gluon distribution in leading order using the BFKL theory [44] result in differences from our $\varphi(x, q^2)$ function given by Eq. (12) by only about 10-15%.

Here we deal with the matrix element accounting for the gluon virtualities and polarizations. Since it is much more complicated than in the parton model we consider only the LO of the subprocess $gg \rightarrow Q\bar{Q}$ which gives the main contribution to the heavy quark production cross section at small x , see the diagrams a, b and c in Fig. 6. The lower and upper ladder blocks present the two-dimensional gluon functions $\varphi(x_1, q_1^2)$ and $\varphi(x_2, q_2^2)$.

Strictly speaking, Eq. (12) may be justified in the leading $\log(1/x)$ limit only. The unintegrated parton distribution $f_a(x, q_T, \mu)$ determines the probability to find a parton a initiating the hard process with the transverse momentum q_T (and with factorization scale μ). To restore the function $f_a(x, q_T, \mu)$ on the basis of the conventional (integrated) parton density $a(x, \lambda^2)$ we have to consider the DGLAP evolution⁵

$$\frac{\partial a}{\partial \ln \lambda^2} = \frac{\alpha_s}{2\pi} \left[\int_x^{1-\Delta} P_{aa'}(z) a'(\frac{x}{z}, \lambda^2) dz - a(x, \lambda^2) \sum_{a'} \int_0^{1-\Delta} P_{a'a}(z') dz' \right] \quad (13)$$

(here $a(x, \lambda^2)$ denotes $xg(x, \lambda^2)$ or $xq(x, \lambda^2)$ and $P_{aa'}(z)$ are the splitting functions).

The first term on the right-hand side of Eq. (13) describes the number of partons δ_a emitted in the interval $\lambda^2 < q_T^2 < \lambda^2 + \delta\lambda^2$, while the second (virtual) term reflects the fact that the parton a disappears after the splitting.

⁵For the $g \rightarrow gg$ splitting we need to insert a factor z' in the last integral of Eq. (13) to account for the identity of the produced gluons.

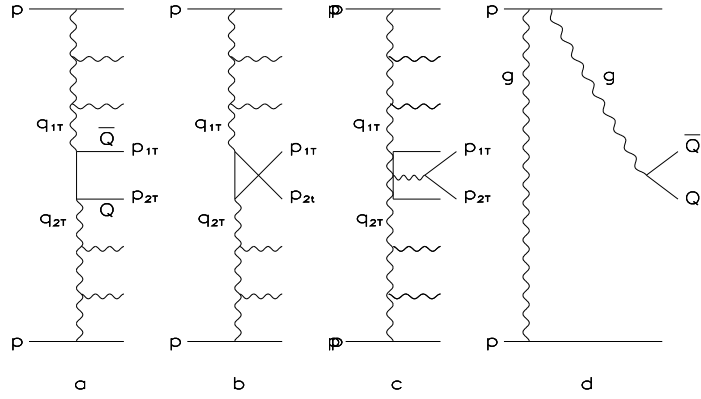


Fig. 6. Low order QCD diagrams for heavy quark production in pp ($p\bar{p}$) collisions via gluon-gluon fusion (a-c) and the diagram (d) formally violating the factorization and being necessary for gauge invariance.

The second contribution may be resummed as giving survival probability T_a that the parton a with the transverse momentum q_T remains untouched in the evolution up to the factorization scale

$$T_a(q_T, \mu) = \exp \left[- \int_{q_T^2}^{\mu^2} \frac{\alpha_s(p_T)}{2\pi} \frac{dp_T^2}{p_T^2} \sum_{a'} \int_0^{1-\Delta} P_{a'a}(z') dz' \right] \quad (14)$$

For the case of one loop QCD running coupling $\alpha_s(p_T) = 4\pi/b \ln p_T^2/\Lambda^2$ the factor $T_a(q_T, \mu)$ can be written down explicitly. In particular, the gluon survival probability (which enters our formulae) reads:

$$\begin{aligned} T_a(q_T, \mu) = \frac{\ln(\mu/\Lambda)}{\ln(q_T/\Lambda)} \cdot \exp \left\{ \frac{8N_c}{b} \left[\ln \frac{\mu}{q_T} - \ln \frac{\mu}{\Lambda} \ln \frac{\ln(\mu/\Lambda)}{\ln(q_T/\Lambda)} - 2E_1(q_T, \mu) + 3/2 E_2(q_T, \mu) - \right. \right. \\ \left. \left. - 2/3 E_3(q_T, \mu) + 1/4 E_4(q_T, \mu) \right] + \right. \\ \left. + \frac{2}{3b} n_F [3E_1(q_T, \mu) - 3E_2(q_T, \mu) + 2E_3(q_T, \mu)] \right\} \end{aligned} \quad (15)$$

where

$$E_k(q_T, \mu) = \left(\frac{\Lambda}{\mu} \right)^k [Ei(k \ln(\mu/\Lambda) - Ei(k \ln(q_T/\Lambda))] , \quad (16)$$

and the integral exponent $Ei(z) = \int_{-\infty}^z \frac{dt}{t} \exp t$; n_F and N_c are the number of light quark flavours and the number of colours, respectively, and $b = 11 - \frac{2}{3}n_F$.

Thus the unintegrated distribution $f_a(x, q_T, \mu)$ reads

$$f_a(x, q_T, \mu) = \left[\frac{\alpha_s}{2\pi} \int_x^{1-\Delta} P_{aa'}(z) a' \left(\frac{x}{z}, q_T^2 \right) dz \right] T_a(q_T, \mu) , \quad (17)$$

where the cut-off $\Delta = q_T/\mu$ is used both in Eqs. (14) and (17) [45, 46].

We have to emphasize that $f_a(x, q_T, \mu)$ is just the quantity which enters into the Feynman diagrams. The distributions $f_a(x, q_T, \mu)$ involve two hard scales⁶: q_T and the scale μ of the probe. The scale μ plays a dual role. On the one hand side it acts as the factorization scale, while on the other hand side it controls the angular ordering of the partons emitted in the evolution [47, 48, 49]. The factorization scale μ separates the partons associated with the emission off both the beam and target protons (in pp collisions) and off the hard subprocess. For example, it separates emissions off the beam (with polar angle $\theta < 90^\circ$ in c.s.m.) from those off the target (with $\theta > 90^\circ$ in c.s.m.), and from the intermediate partons from the hard subprocess. This separation was proved in [47, 48, 49] and originates from the destructive interference of the different emission amplitudes (Feynman diagrams) in the angular boundary regions.

If the longitudinal momentum fraction is fixed by the hard subprocess, then the limits of the angles can be expressed in terms of the factorization scale μ which corresponds to the upper limit of the allowed value of the s -channel parton k_T .

⁶This property is hidden in the conventional parton distributions as q_T is integrated up to the scale μ .

Since the parton distributions contain two scales, one has to deal with a complicated evolution equation for $f_a(x, q_T, \mu)$. On the other hand since the evolution is controlled by the emission angle only, the distribution $f_a(x, q_T, \mu)$ can be obtained from a single scale evolution equation, as it was done in Eq. (17).

In the leading $\log(1/x)$ (i.e. BFKL) limit the virtual DGLAP contribution is neglected. So $T_a = 1$ and one comes back to Eq. (12)

$$f_a^{BFKL}(x, q_T, \mu) = \frac{\partial a(x, \lambda^2)}{\partial \ln \lambda^2} \Big|_{\lambda = q_T} . \quad (18)$$

In the double log limit Eq. (17) can be written in the form

$$f_a^{DDT}(x, q_T, \mu) = \frac{\partial}{\partial \ln \lambda^2} \left[a(x, \lambda^2) T_a(\lambda, \mu) \right]_{\lambda = q_T} , \quad (19)$$

which was firstly proposed by [50]. In this limit the derivative $\partial T_a / \partial \ln \lambda^2$ cancels the second term of the r.h.s. of Eq. (13) (see [46] for a more detailed discussion).

Finally, the probability $f_a(x, q_T, \mu)$ is related to the BFKL function $\varphi(x, q_T^2)$ by

$$\varphi(x, q^2) = 4\sqrt{2}\pi^3 f_a(x, q_T, \mu) . \quad (20)$$

Note that due to a virtual DGLAP contribution the derivative $\partial a(x, \lambda^2) / \partial \lambda^2$ can be negative for not small enough x values. This shortcoming of Eq. (18) is partly overcome in the case of Eq. (19). Unfortunately the cut-off Δ used in a conventional DGLAP computation does not depend on the scale μ . To obtain an integrated parton distributions it is enough to put any small $\Delta \ll 1^7$.

On the other hand, in the survival probability Eq. (14) we have to use the true (within the leading log approximation) value $\Delta = q_T / \mu$. Hence for a rather large q_T ($\sim \mu$) and x even the DDT form Eq. (19) is not precise. Only the expression (17) with the same cut-off Δ in a real DGLAP contribution and in the survival probability (14) provides the positivity of the unintegrated probability $f_a(x, q_T, \mu)$ in the whole interval $0 < x < 1$.

Of course, just by definition $f_a(x, q_T, \mu) = 0$ when the transverse momentum q_T becomes larger than the factorization scale μ .

In what follows we use the Sudakov decomposition for the quark momenta $p_{1,2}$ through the momenta of colliding hadrons p_A and p_B ($p_A^2 = p_B^2 \simeq 0$) and the transverse momenta $p_{1,2T}$:

$$p_{1,2} = x_{1,2} p_B + y_{1,2} p_A + p_{1,2T} . \quad (21)$$

⁷There is a cancellation between the real and virtual soft gluon DL contributions in the DGLAP equation, written for the integrated partons (including all $k_T \leq \mu$). The emission of a soft gluon with momentum fraction $(1-z) \rightarrow 0$ does not affect the x -distribution of parent partons. Thus the virtual and real contributions originated from $1/(1-z)$ singularity of the splitting function $P(z)$ cancel each other.

On the contrary, in the unintegrated case the emission of soft gluon (with $q'_T > k_T$) alters the transverse momentum of parent (t -channel) parton. Eq. (17) includes this effect through the derivative $\partial T(k_T^2, \mu^2) / \partial k_T^2$.

The differential cross section of heavy quark hadroproduction has the following form:⁸

$$\begin{aligned} \frac{d\sigma_{pp}}{dy_1^* dy_2^* d^2p_{1T} d^2p_{2T}} &= \frac{1}{(2\pi)^8} \frac{1}{(s)^2} \int d^2q_{1T} d^2q_{2T} \delta(q_{1T} + q_{2T} - p_{1T} - p_{2T}) \\ &\times \frac{\alpha_s(q_1^2)}{q_1^2} \frac{\alpha_s(q_2^2)}{q_2^2} \varphi(q_1^2, y) \varphi(q_2^2, x) |M_{QQ}|^2. \end{aligned} \quad (22)$$

Here $s = 2p_{ApB}$, $q_{1,2T}$ are the gluon transverse momenta and $y_{1,2}^*$ are the quark rapidities in the hadron-hadron c.m.s. frame,

$$\begin{aligned} x_1 &= \frac{m_{1T}}{\sqrt{s}} e^{-y_1^*}, & x_2 &= \frac{m_{2T}}{\sqrt{s}} e^{-y_2^*}, & x &= x_1 + x_2 \\ y_1 &= \frac{m_{1T}}{\sqrt{s}} e^{y_1^*}, & y_2 &= \frac{m_{2T}}{\sqrt{s}} e^{y_2^*}, & y &= y_1 + y_2 \\ m_{1,2T}^2 &= m_Q^2 + p_{1,2T}^2. \end{aligned} \quad (23)$$

$|M_{QQ}|^2$ is the square of the matrix element for the heavy quark pair hadroproduction. Contrary to the mention of [24], the transformation Jacobian from x, y to y_1^*, y_2^* is accounted in our matrix element.

In LLA kinematic

$$q_1 \simeq y p_A + q_{1T}, \quad q_2 \simeq x p_B + q_{2T}. \quad (24)$$

so

$$q_1^2 \simeq -q_{1T}^2, \quad q_2^2 \simeq -q_{2T}^2. \quad (25)$$

(The more accurate relations are $q_1^2 = -\frac{q_{1T}^2}{1-y}$, $q_2^2 = -\frac{q_{2T}^2}{1-x}$ but we are working in the kinematics where $x, y \ll 1$).

The matrix element M is calculated in the Born approximation of QCD without standard simplifications of the parton model.

In the axial gauge $p_B^\mu A_\mu = 0$ the gluon propagator takes the form $D_{\mu\nu}(q) = d_{\mu\nu}(q)/q^2$,

$$d_{\mu\nu}(q) = \delta_{\mu\nu} - (q^\mu p_B^\nu + q^\nu p_B^\mu)/(p_B q). \quad (26)$$

For the gluons in t -channel the main contribution comes from the so called "non-sense" polarization $g_{\mu\nu}^n$, which can be picked out by decomposing the numerator into longitudinal and transverse parts:

$$\delta_{\mu\nu}(q) = 2(p_B^\mu p_A^\nu + p_A^\mu p_B^\nu)/s + \delta_{\mu\nu}^T \approx 2p_B^\mu p_A^\nu/s \equiv g_{\mu\nu}^n. \quad (27)$$

The other contributions are suppressed by the powers of s . It is easy to check that in axial gauge (26) $p_B^\mu d_{\mu\nu} = 0$ and $p_A^\mu d_{\mu\nu} \simeq -q_T^\nu/y$. Thus we effectively get

$$d_{\mu\nu}(q) \approx -2 \frac{p_B^\mu q_T^\nu}{y s}. \quad (28)$$

⁸We put the argument of α_s to be equal to gluon virtuality, which is very close to the BLM scheme[51]; (see also [21]).

Another way to obtain the same result is to use the transversality condition. Since the sum of the diagram Fig. 6a-c is gauge invariant (see below) the product $q_{1\mu}M_\mu = 0$, here M_μ denotes the amplitude of the gluon q_1 and hadron p_B interaction described by the lower part of Fig. 6a-c. Using the expansion (24) for the q_1 momentum we obtain

$$p_A^\mu M_\mu \simeq -\frac{q_{1T}^\mu}{y} M_\mu ,$$

which leads to Eq. (28) or

$$d_{\mu\nu}(q) \approx 2 \frac{q_T^\mu q_T^\nu}{xys} , \quad (29)$$

if we do such a trick for the vector p_B too ⁹. Both these equations for $d_{\mu\nu}$ can be used but for the form (28) one has to modify the gluon vertex slightly (to account for several ways of gluon emission – see ref. [22]):

$$\Gamma_{eff}^\nu = \frac{2}{xys} \left[(xys - q_{1T}^2) q_{1T}^\nu - q_{1T}^2 q_{2T}^\nu + 2x (q_{1T} q_{2T}) p_B^\nu \right] . \quad (30)$$

As a result the colliding gluons can be treated as aligned ones and their polarization vectors are directed along the transverse momenta. Ultimately, the nontrivial azimuthal correlations must arise between the transverse momenta p_{1T} and p_{2T} of the heavy quarks.

From the formal point of view there is a danger to loose the gauge invariance in dealing with the off mass shell gluons. Say, in the covariant Feynman gauge the new graphs (similar to the "bremsstrahlung" from the initial or final quark line, as it is shown in Fig. 6d) may contribute in the central plato rapidity region. However this is not the fact. Within the "semihard" accuracy, when the function $\varphi(x, q^2)$ collects the terms of the form $\alpha_s^k (\ln q^2)^n (\ln(1/x))^m$ with $n + m \geq k$, the triple gluon vertex (30) includes effectively all the leading logarithmic contributions of the Fig. 6d type [44, 20]. For instance, the upper part of the graph shown in Fig. 6d corresponds in terms of the BFKL equation to the t -channel gluon reggeization. Thus the final expression is gauge invariant (except a small, non-logarithmic, $O(\alpha_s)$ corrections) ¹⁰.

Although the situation considered here seems to be quite opposite to the parton model there is a certain limit [22], in which our formulae can be transformed into parton model ones, namely when the quark transverse momenta, $p_{1,2T}$, are much larger than the gluon ones, $q_{1,2T}$.

⁹Having in mind this trick one can say that the matrix element is gauge-invariant in the k_T -factorization approach. However the polarization vectors of incoming gluons q_1 and q_2 are not arbitrary taken but fixed as $-q_{1T}^\mu/y$ and $-q_{2T}^\nu/x$, respectively (see [18] for more detail).

¹⁰Taking the gluon polarization vector as $-q_{1T}^\mu/y$ we can completely eliminate the leading logarithm terms arising from Fig. 6d.

4 Qualitative difference between k_T -factorization approach and parton model

Eq. (22) enables to calculate straightforwardly all distributions concerning one-particle or pair production. To illustrate the difference between our approach and the conventional parton model we present first of all the results of calculations of charm production ($m_c = 1.4$ GeV [33, 34]) with high p_T at three energies, $\sqrt{s} = 1$ TeV, 10 TeV and 10^3 TeV and with the same value of

$$x_T = \frac{2p_T}{\sqrt{s}} = 0.02, \quad (31)$$

i.e. $p_T = 10$ GeV, 100 GeV and 10^4 GeV for the above energies.

We will use QCD scales $\mu_F = m_T = \sqrt{m_c^2 + p_T^2}$ and $\mu_R = m_c$, i.e. fixed coupling with $N_f = 3$ and $\Lambda = 248$ MeV [30].

However there exists a problem coming from the infrared region, because the functions $\varphi(x, q_2^2)$ and $\varphi(y, q_1^2)$ are unknown at the small values of $q_{1,2}^2$. Moreover, for the realistic gluon structure functions the value $\varphi(x, q^2)$ is positive in the small- x region and negative in the large- x region. The boundary between two regions, where $\varphi(x, q^2) = 0$, depends on the q^2 , therefore the relative contributions of these regions is determined by the characteristic scale of the reaction, say, by the transverse momentum p_T .

To avoid this additional problem, we present the numerical calculations both in the k_T -factorization approach and in the LO parton model, using the "toy" gluon distribution

$$xG(x, q^2) = (1-x)^5 \ln(q^2/Q_0^2), \quad (32)$$

for $q^2 > Q_0^2$, and $xG(x, q^2) = 0$ for $q^2 < Q_0^2$, with $Q_0^2 = 1$ GeV².

After the calculations of charm production cross sections using, say, the VEGAS code [52] (that is the optimized Monte Carlo program for integrating the multidimensional expressions) and with Eqs. (12), (22), (32) one can see, that the values $d\sigma/dx_T$ at $x_T = 0.02$ are about 4–5 times larger in the k_T -factorization approach than in the LO parton model, Eq. (1). Really this difference should not be considered as very large because, as it was discussed, an essential part of NLO and NNLO corrections is already included in the k_T -factorization, and it is known that the sum of the LO and NLO contributions in the parton model is about 2-3 times larger than the LO contribution [55].

To show the most important values of the variables $q_{1,2T}$ in Eq. (22), as well as the kinematical region producing the main difference with the conventional parton model, we plot by dots in Fig. 7 the results of the k_T -factorization approach with the restrictions $|q_{1,2T}| \leq q_{max}$, as a function of q_{max} . The running coupling is fixed as $\alpha_S(m_c^2)$ instead of $\alpha_S(q_{1,2}^2)$ in Eq. (22). The dashed lines in Fig. 7 are the conventional parton model predictions with QCD scales $\mu_F = \sqrt{m_c^2 + p_T^2}$, and $\mu_R = m_c$. One can see that the k_T -factorization predictions exceed the parton model results when $q_{max} \geq p_T$.

Let us check now that the k_T -factorization predictions really coincide with the parton model ones when the quark momenta, $p_{1,2T}$, are much larger than the gluon momenta,

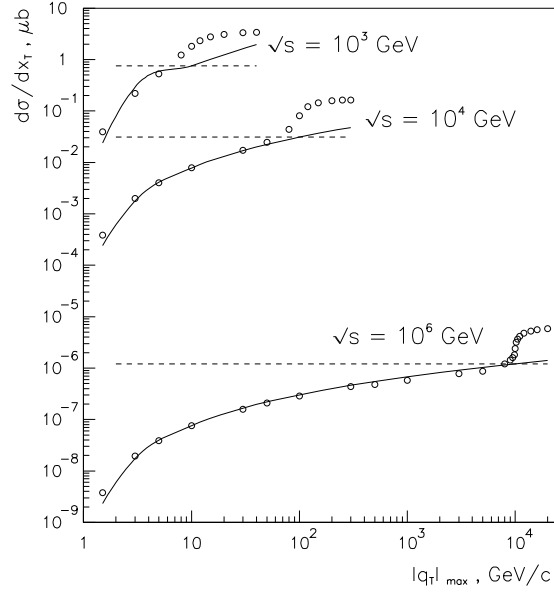


Fig. 7. The values of $d\sigma/dx_T$ for charm hadroproduction at $x_T = 0.02$ in k_T -factorization approach as a function of upper limits of integrals in Eq. (22) (points); the conventional parton model values (dashed lines) and the values of right-hand side of Eq. (34) (solid curves).

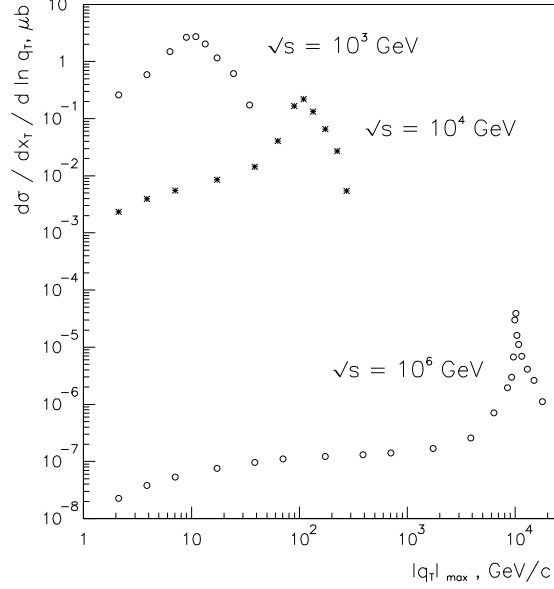


Fig. 8. The values of $d\sigma/dx_T/d \ln q_{max}$ for charm hadroproduction at $x_T = 0.02$ in k_T -factorization approach as a function of upper limits of integrals in Eq. (22) (points).

$q_{1,2T}$ [22]. However we have to compare them at the same values of structure functions. When we submit Eq. (22) to the conditions $|q_{1,2T}| \leq q_{max}$ and neglect the $q_{1,2T}$ dependence in the matrix element, we recover the parton model approximation, and get the result proportional to $xG(x, q_{max}^2) \cdot yG(y, q_{max}^2)$ due to the direct consequence of Eq. (12) [53]

$$xG(x, q^2) = xG(x, Q_0^2) + \frac{1}{4\sqrt{2}\pi^3} \int_{Q_0^2}^{q^2} \varphi(x, q_1^2) dq_1^2. \quad (33)$$

At the same time the original parton model yields the result proportional to $xG(x, \mu_F^2) \cdot yG(y, \mu_F^2)$ with $\mu_F = \sqrt{m_c^2 + p_T^2}$. Hence we expect the parton model to coincide with our calculations for the gluon distribution Eq. (32), $p_T \gg m_c$ and $|q_{1,2T}| \leq q_{max}$ after multiplying by an appropriate factor:

$$\left. \frac{d\sigma}{dx_T} \right|_{q_{iT} \ll p_{iT}} = \left. \frac{d\sigma}{dx_T} \right|_{PM} \left(\frac{\ln(q_{max}^2/Q_0^2)}{\ln(p_T^2/Q_0^2)} \right)^2. \quad (34)$$

The right-hand side of Eq. (34) presented in Fig. 7 by solid curves shows a good agreement with k_T -factorization approach (open dots) even when q_{max} is only slightly smaller (at the highest energy) than p_T . The same values $d\sigma/dx_T$, as in Fig. 7, but differentiated with respect to $\ln q_{max}$ are presented in Fig. 8 for k_T -factorization approach. It exhibits, especially at the high energies, the logarithmic growth with q_{max} , until the

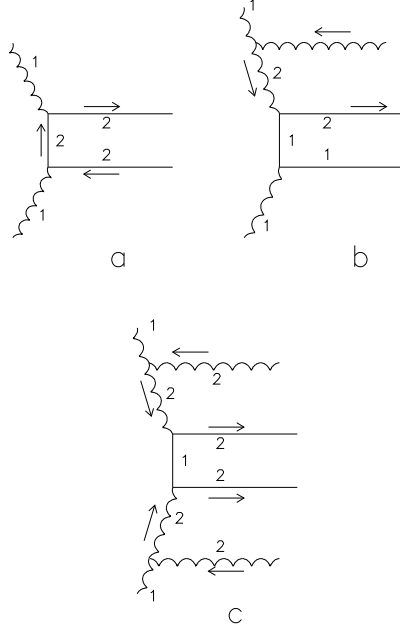


Fig. 9. The diagrams which are important in the case of one-particle distributions of heavy quark with large p_T . High p_T flows are shown by arrows. The situation similar to the LO parton model (a). The case, possible in NLO parton model, large p_T of the quark is compensated by hard gluon and the fermion propagator is near to mass shell (b). The numerically small contribution, when large transverse momenta of heavy quarks are compensated by two hard gluons, whereas the fermion propagator is near to mass shell (c).

value $q_{max} \sim p_T$. There is the narrow peak in this region, which provides about 70-80 % of the $d\sigma/dx_T$ cross section integrated over the whole $q_{1,2T}$ phase space. Its physical nature seems to be quite clear. There are two kinematical regions for t -channel and u -channel diagrams, Fig. 6 a,b, giving comparatively large contributions to $d\sigma/dx_T$ for the high energies and high p_T heavy quark production. One of them comes from the conventional parton model kinematics when both initial gluon transverse momenta, $q_{1,2T}$, are very small compared to $p_{1,2T}$, see Fig. 9a. Another large contribution appears from the region where, say, $q_{1T} \sim p_{1T}$, whereas q_{2T} and p_{2T} are comparatively small, as it is shown in Fig. 9b. In this case the quark propagator, $1/(\hat{p}_1 - \hat{q}_1 - m_Q) = 1/(\hat{q}_2 - \hat{p}_2 - m_Q)$, is close to the mass shell and gives rise to the narrow peak shown in Fig. 8. The general smallness of such processes comes from high-virtuality gluon propagator in Fig. 9b, and it is of the same order as in the case of Fig. 9a, despite the diagram Fig. 9a is suppressed by the fermion propagator for the large rapidity difference between the two produced heavy quarks.

The diagram shown in Fig. 9b can be considered [1] as one of the most important contribution to the NLO parton model in the high energy limit, because of spin-one

Table 1: The ratios of $c\bar{c}$ pair production in k_T -factorization approach and in LO parton model

\sqrt{s} , TeV	0.3	1	10	100	1000
R_{tot}	4.0	4.0	4.0	3.9	3.9
$R(x_T = 0.02)$	3.4	4.5	5.5	5.4	5.2

gluon exchange in the t -channel. Due to these factors, combinatorics and interference between diagrams, the resulting k_T -factorization contribution to the peak at $q_T \sim p_T$ in the total $d\sigma/dx_T$ value in Fig. 8 is several times larger than the LO parton model contribution. In the Table 1 we present the calculated ratios of the total heavy quark pair production cross section, R_{tot} , and the ratio of $d\sigma/dx_T$, $R(x_T)$ at $x_T = 0.02$ (integrated over rapidity).

One can see that at fixed x_T the relative contribution of the discussed peaks at first increases due to increase of the phase space. This contribution is saturated at the high enough energy ($\sqrt{s} \sim 10$ TeV). After this the relative contribution of the LO parton model increases logarithmically with p_T , and have to dominate at the extremely high energies and p_T , in academical asymptotic.

These results are confirmed by those presented in Fig. 10, where we reproduce the data from Fig. 7 for LO parton model and k_T -factorization approach with the condition $|q_{1,2T}| \leq q_{max}$. For comparison we show by stars the k_T -factorization predictions for all values q_{1T} with the only condition $|q_{2T}| \leq q_{max}$, versus q_{max} . The last results are above the LO parton model even at not too large q_{2T} because the peaks, discussed above, are included into the integral over q_{1T} .

Let us note that the calculation of $d\sigma/dx_T$ at $\sqrt{s} = 10$ TeV, $x_T = 0.02$, and with restriction $|q_{1,2T}| \geq p_T/2$ (see Fig. 9c) gives only about 2% of the total value of $d\sigma/dx_T$.

The essential values of $q_{1,2T}$ increase in our calculations when the transverse momentum, p_T of the detected c -quark increases. At the high initial energy $q_{1,2T} \sim p_T$. In the k_T kick language it means that the $\langle k_T^2 \rangle$ value also increases.

5 Total cross sections and one-particle distributions

Eq. (22) enables us to calculate straightforwardly all distributions concerning one-particle or pair production. One-particle calculations as well as correlations between two produced heavy quarks can be easily done using, say, the VEGAS code [52].

However there exists a principle problem coming from the infrared region. Since the functions $\varphi(x, q_2^2)$ and $\varphi(y, q_1^2)$ are unknown at small values of q_2^2 and q_1^2 , i.e. in

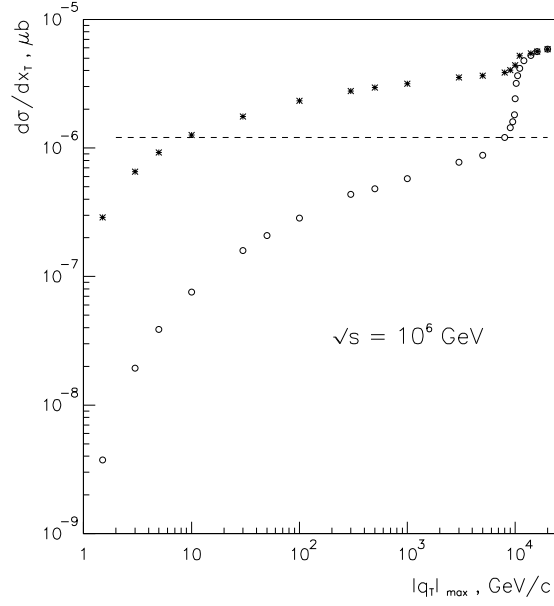


Fig. 10. The same as in Fig. 7 (points and dashed curves) together with the values of $d\sigma/dx_T$ (stars) for the case when only q_{2T} upper limit integration is bounded by q_{max} .

nonperturbative domain we use Eq. (33) and rewrite the integrals in the Eq. (22) as

$$\begin{aligned}
& \int d^2 q_{1T} d^2 q_{2T} \delta(q_{1T} + q_{2T} - p_{1T} - p_{2T}) \frac{\alpha_s(q_1^2)}{q_1^2} \frac{\alpha_s(q_2^2)}{q_2^2} f_g(y, q_{1T}, \mu) f_g(x, q_{2T}, \mu) |M_{QQ}|^2 = \\
& = (4\sqrt{2} \pi^3 \alpha_s(m_T^2))^2 x G(x, Q_0^2) y G(y, Q_0^2) T^2(Q_0^2, \mu^2) \left(\frac{|M_{QQ}|^2}{q_1^2 q_2^2} \right)_{q_{1,2} \rightarrow 0} + \quad (35) \\
& + 4\sqrt{2} \pi^3 \alpha_s(m_T^2) x G(x, Q_0^2) T(Q_0^2, \mu^2) \int_{Q_0^2}^{\infty} dq_{1T}^2 \delta(q_{1T} - p_{1T} - p_{2T}) \times \\
& \quad \times \frac{\alpha_s(q_1^2)}{q_1^2} f_g(y, q_{1T}, \mu) \left(\frac{|M_{QQ}|^2}{q_2^2} \right)_{q_2 \rightarrow 0} + \\
& + 4\sqrt{2} \pi^3 \alpha_s(m_T^2) y G(y, Q_0^2) T(Q_0^2, \mu^2) \int_{Q_0^2}^{\infty} dq_{2T}^2 \delta(q_{2T} - p_{1T} - p_{2T}) \times \\
& \quad \times \frac{\alpha_s(q_2^2)}{q_2^2} f_a(x, q_{2T}, \mu) \left(\frac{|M_{QQ}|^2}{q_1^2} \right)_{q_1 \rightarrow 0} + \\
& + \int_{Q_0^2}^{\infty} d^2 q_{1T} \int_{Q_0^2}^{\infty} d^2 q_{2T} \delta(q_{1T} + q_{2T} - p_{1T} - p_{2T}) \times \\
& \quad \times \frac{\alpha_s(q_1^2)}{q_1^2} \frac{\alpha_s(q_2^2)}{q_2^2} f_g(y, q_{1T}, \mu) f_g(x, q_{2T}, \mu) |M_{QQ}|^2,
\end{aligned}$$

where the unintegrated gluon distributions $f_g(x, q_T, \mu)$ are taken from Eqs. (14) and (17). In the numerical calculations we use the values $\mu^2 = \hat{s}$ and $\mu^2 = \hat{s}/4$.

The first contribution in Eq. (35) with the matrix element averaged over directions of the two-dimensional vectors q_{1T} and q_{2T} is exactly the same as the conventional LO parton model expression. It is multiplied by the 'survival' probability $T^2(Q_0^2, \mu^2)$ not to have transverse momenta $q_{1T}, q_{2T} > Q_0$. The QCD scales are $\mu_R^2 = m_T^2$ and $\mu_F^2 = Q_0^2$ (the same value as in Eq. (33), we assume $Q_0^2 = 1 \text{ GeV}^2$) The sum of the produced heavy quark momenta is taken to be exactly zero here.

The next three terms contain the corrections to the parton model due to gluon polarizations, virtualities and transverse momenta in the matrix element. The relative contribution of the corrections strongly depends on the initial energy. If it is not high enough, the first term in Eq. (35) dominates, and all results are similar to the conventional LO parton model predictions. In the case of very high energy the opposite situation takes place, the first term in Eq. (35) can be considered as a small correction and our results differ from the conventional ones. It is necessary to note that the absolute as well as the relative magnitudes of all the pieces in Eq. (35) strongly depend on the T-factor (i.e., when we use Eq. (17) or Eq. (12)).

Before the numerical comparison it is necessary to remind that the NLO parton model actually results only in a normalization factor in the case of one-particle distributions, the shapes of LO and LO+NLO distributions are almost the same [3, 4, 5, 54], see Fig. 2. This means that we can calculate the K-factor Eq. (7), say, from the results for the total production cross sections, and restrict ourselves only to the LO calculations of p_T or rapidity distributions multiplying them by the K-factors.

The numerical values of the K-factors depend [55] on the structure functions used, quark masses, QCD scales and the initial energy, the renormalization scale μ_R being especially important. This seems to be evident, because the LO contribution is proportional to α_S^2 , whereas the NLO contribution is proportional to α_S^3 . However the structure of Eq. (2) is more important at the high energies, when small ρ values dominate. At $\rho \rightarrow 0$ the functions $f_{gg}^{(1)}$ and $\bar{f}_{gg}^{(1)}$ have the constant limits [1], $f_{gg}^{(1)}(\rho \rightarrow 0) \approx 0.1$ and $\bar{f}_{gg}^{(1)}(\rho \rightarrow 0) \approx -0.04$, while $f_{gg}^{(0)}(\rho \rightarrow 0) \rightarrow 0$. Therefore due to Eq. (2) the K factor value at the high energies is mainly determined by the ratio μ/m_Q .

First of all let us present the role of the T-factors, Eq. (14). In Fig. 11 we show the ratios of the last term of Eq. (35) with the T-factors in both gluon distributions $f_g(x, q_{iT}, \mu)$ to the same values calculated for $T_g(x, q_{1T}, \mu) = 1$ in one unintegrated gluon distribution. The ratios are plotted as functions of q_{1T} for the cases of charm and beauty production at $\sqrt{s} = 14 \text{ TeV}$ and $\mu^2 = \hat{s}$. The heavy quark transverse momenta are fixed to be $20 \text{ GeV}/c$. In both cases the factors $T_a(q_{1t})$ are rather small at small q_{1T} and $T_g(x, q_{1T}, \mu) \rightarrow 1$ at $p_T \gg q_{1T}$.

Now let us compare the numerical results predicted by the parton model and by the k_T -factorization approach.

The energy dependences of the total cross sections of $c\bar{c}$ and $b\bar{b}$ pair production are presented in Fig. 12. As was mentioned, at comparatively small energies the first

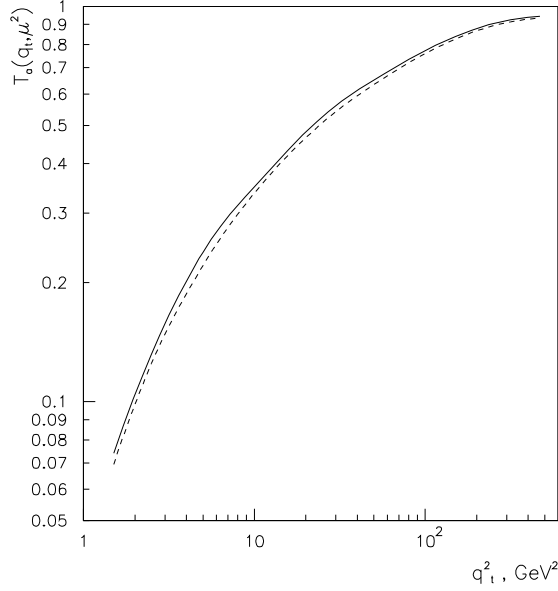


Fig. 11. The role of T -factor, Eq. (14) in the calculation of charm (solid curve) and beauty (dashed curve) production with $p_T = 20$ GeV/c at $\sqrt{s} = 14$ TeV and $\mu^2 = \hat{s}$.

term in Eq. (35) dominates and the results of the k_T -factorization approach should be close to the LO parton model prediction. Actually the first results are even smaller due to the presence of the T -factor in Eq. (17). However the k_T -factorization approach yields a stronger energy dependence than the LO parton model both for $c\bar{c}$ and $b\bar{b}$ production. This can be explained by additional contributions appearing at very high energies in the k_T -factorization approach when the transverse momentum of a heavy quark is compensated by the nearest gluon, see [28]

One-particle p_T distributions, $d\sigma/dp_T$, calculated in the k_T -factorization approach and in the LO parton model are presented in Fig. 13. In all cases the k_T -factorization predicts broader distributions. The average values of p_T of the produced heavy quarks are rather different in these two approaches, as one can see from Table 2.

Table 2 The average values of charm and beauty quark transverse momenta $\langle p_T \rangle$ (in GeV/c) in the k_T -factorization approach with $\mu^2 = \hat{s}$ and in the LO parton model.

	LO parton model		k_T -factorization	
\sqrt{s}	$c\bar{c}$	$b\bar{b}$	$c\bar{c}$	$b\bar{b}$
14 TeV	1.78	4.53	2.23	5.47
1.8 TeV	1.48	3.96	1.91	4.54

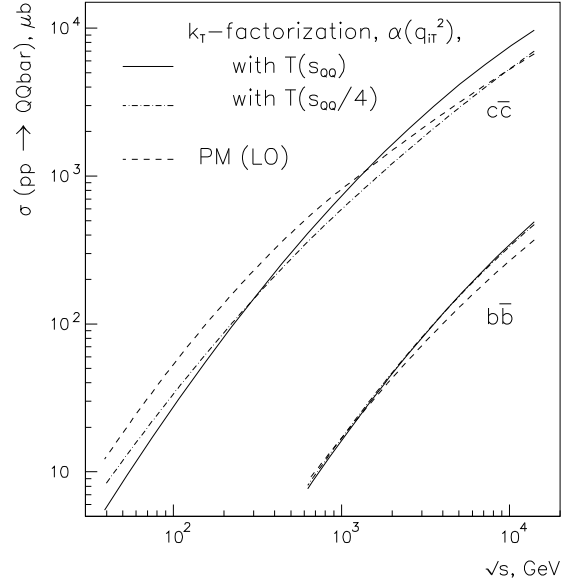


Fig. 12. The total cross sections for charm and beauty hadroproduction in the k_T -factorization approach with unintegrated gluon distribution $f_g(x, q_T, \mu)$ given by Eq. (17), for μ^2 values in Eq. (14) equal to \hat{s} (solid curves), and $\hat{s}/4$ (dash-dotted curves), and in the LO parton model (dashed curves).

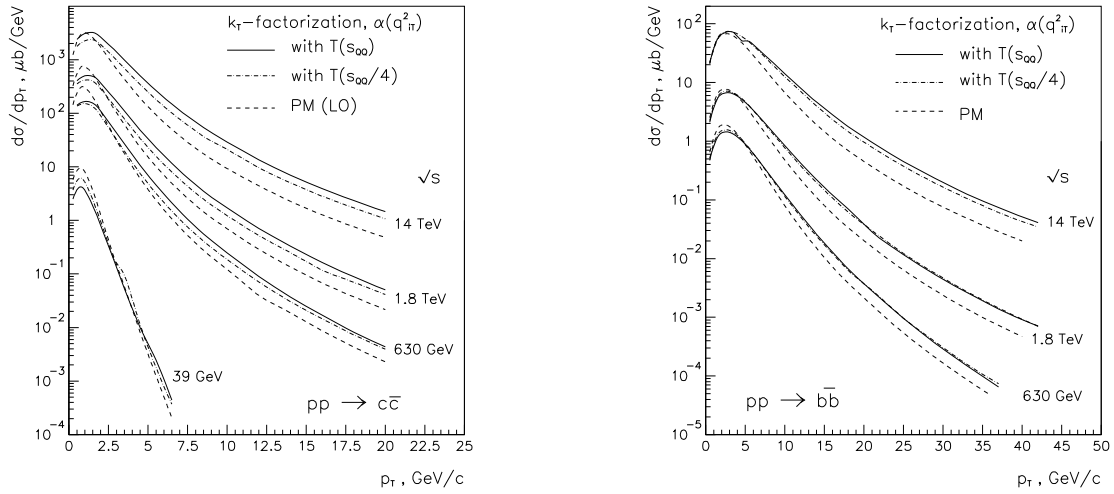


Fig. 13. p_T -distributions of c -quarks (a) and b -quarks (b) produced at different energies. Dashed curves are the results of the LO parton model. Solid curves are calculated with the unintegrated gluon distribution $f_g(x, q_T, \mu)$ given by Eq. (17), for μ^2 values in Eq. (14) equal to \hat{s} and dash-dotted curves are calculated for $\mu^2 = \hat{s}/4$.

This seems to be very natural, because, contrary to the LO parton model, a large p_T of the one heavy quark can be compensated not only by the p_T of the other heavy quark but also by neighbour gluons emission, Fig. 9b.

The rapidity distributions of produced heavy quarks presented in Fig. 14 show that the main part of the difference between the k_T -factorization approach and the LO parton model comes from the central region.

6 Two-particle correlations

We saw from the previous section that there is not so large difference in our results for the total cross sections and one-particle distributions obtained in the k_T -factorization and in the LO parton model. The predictions of the NLO parton model for these quantities differ from the LO parton model only by a normalization factor of 2-2.5 [3, 4, 5, 54]. Hence the difference between our predictions and the NLO parton model should be small.

The calculations of two-particle correlations in different approaches are more informative. The simplest and/or most informative correlation here is the distribution of the total transverse momentum of the produced heavy quark pair, p_{pair} . In the LO parton model $p_{pair} = p_{1T} + p_{2T} = q_{1T} + q_{2T}$, therefore if $q_{1T} = q_{2T} = 0$, then $d\sigma/dp_{pair}$ is a δ -function with $p_{pair} = 0$. Thus the p_{pair} distributions provide the direct information

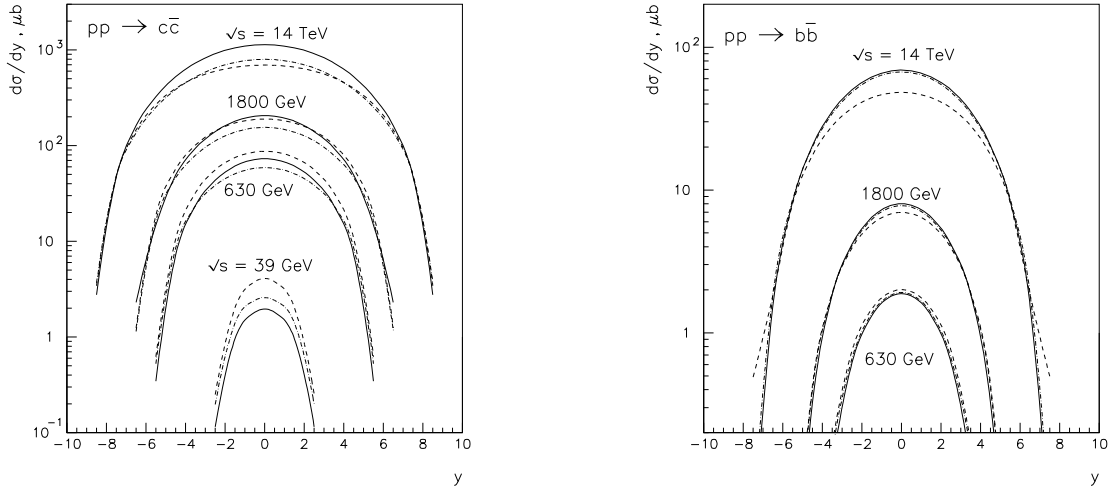


Fig. 14. Rapidity distributions of c -quarks (a) and b -quarks (b) produced at different energies. Dashed curves are the results of the LO parton model. Solid curves are calculated with the unintegrated gluon distribution $f_g(x, q_T, \mu)$ given by Eqs. (17), for μ^2 values in Eq. (14) equal to \hat{s} and dash-dotted curves are calculated for $\mu^2 = \hat{s}/4$.

about the transverse momentum distribution of the incident partons.

It is clear that if $q_{iT} \ll p_{iT}$, then the distributions in p_{pair} should be narrower in comparison with the one-particle p_T distributions. In this case the Weizsaecker-Williams approximation should be valid and one can believe that the parton model reflects the real dynamics of the interaction. In the opposite case, $q_{iT} \sim p_{iT}$, the large transverse momentum of the produced heavy quark can be compensated not by the other quark, but by a high- p_T gluon. We have shown [28] (see Sect. 4), that about 70-80% of the total cross section of high- p_T quark production at high energies originates from such processes, when the heavy quark propagator is close to the mass shell.

We calculate the values of $d\sigma/dp_{pair}$ for charm (a) and beauty (b) production in the k_T -factorization approach using the unintegrated gluon distribution Eqs. (14), (17) with scale values $\mu^2 = \hat{s}$ and $\mu^2 = \hat{s}/4$ (the last value only for $\sqrt{s} = 14$ TeV). Our results for pair production at different initial energies are shown by solid curves in Fig. 15. For the comparison we present by dashed curves the one-particle p_T -distributions taken from Fig. 13, obtained in the same k_T -factorization approach and with the same T -factor. As we put $Q_0^2 = 1$ GeV² in Eq. (35), we can not distinguish between the initial gluons with q_T equal to, say, 0.1 GeV/c and 0.9 GeV/c, so our first bin in the $d\sigma/dp_{pair}$ distribution has the width 2 GeV/c which explains some irregular behaviour of the solid curves at the small p_T . Naturally, all the solid and dashed curves are equally normalized at the same energy.

At comparatively small energies, $\sqrt{s} = 39$ GeV and even at $\sqrt{s} = 630$ GeV the

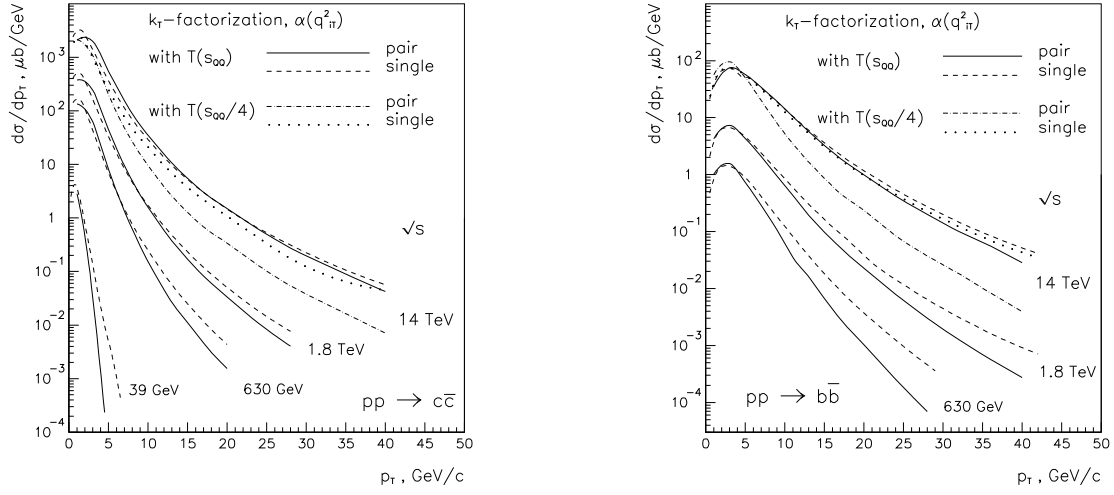


Fig. 15. The distributions of the total transverse momentum p_{pair} for c -quarks (a) and b -quarks (b) produced at different energies (solid curves), calculated with the unintegrated gluon distribution $f_g(x, q_T, \mu)$ given by Eq. (14) and (17), for μ^2 values in Eq. (14) equal to \hat{s} . Dashed curves show the one-particle (single) p_T -distributions with the same μ^2 taken from Fig. 13. Dash-dotted and dotted curves are the same calculations for pair and single production at $\sqrt{s} = 14$ TeV with $\mu^2 = \hat{s}/4$.

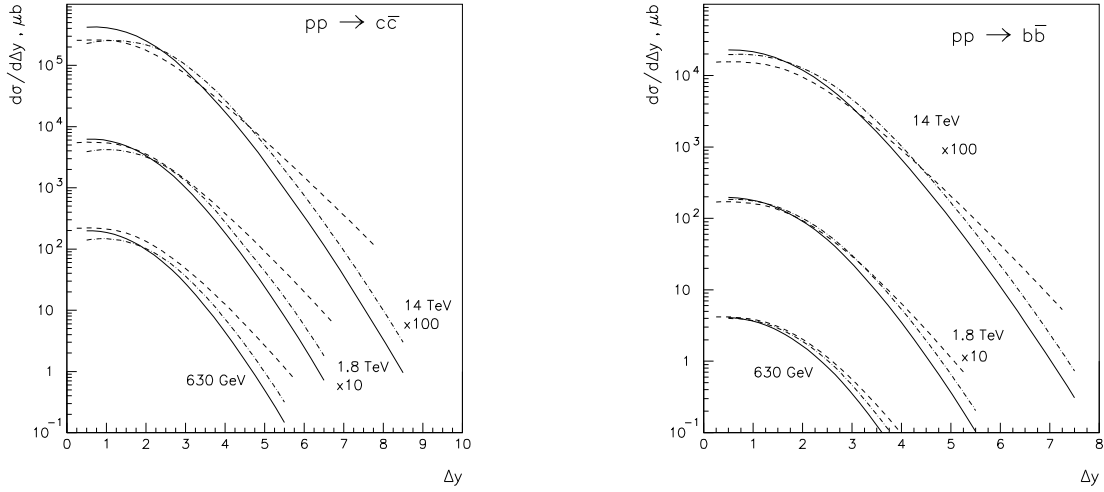


Fig. 16. The calculated distributions of the rapidity difference between two c -quarks (a) or b -quarks (b) produced at different energies in the k_T factorisation approach, calculated with unintegrated gluon distribution $f_g(x, q_T, \mu)$ given by Eq. (17), for μ^2 values in Eq. (14) equal to \hat{s} (solid curves) and $\mu^2 = \hat{s}/4$ (dash-dotted curves). Dashed curves show the LO PM predictions.

distributions $d\sigma/dp_{pair}$ are narrower than the one-particle distributions $d\sigma/dp_T$. This means that the transverse momenta of the produced heavy quarks almost completely compensate each other. However the situation changes drastically with increasing of the initial energy. Starting from comparatively small p_T , the difference between the curves decreases with energy. At $\sqrt{s} = 14$ TeV the distributions are similar both in the cases of $c\bar{c}$ and $b\bar{b}$ production. This means that the production mechanism changes in the discussed energy region. At $\sqrt{s} = 14$ TeV the transverse momentum of the produced heavy quark is balanced more probably by one or several gluons, because the contribution with large virtuality in the quark propagator is more suppressed in comparison with the large virtuality in the gluon propagator.

The discussed behaviour depends on the value of the scale μ^2 in the T -factor, Eq. (14). The similar calculation at energy $\sqrt{s} = 14$ TeV with $\mu^2 = \hat{s}/4$ is shown in Fig. 15 for pair and single production by dash-dotted and dotted curves, respectively. Here the difference between these two curves is more significant and becomes larger for lower energies.

The distributions of the produced heavy quark pair as a function of the rapidity gap $\Delta y = |y_Q - y_{\bar{Q}}|$ between quarks are presented in Figs. 16. Difference between the LO PM and the k_T -factorization predictions is not large again except for the region of very large Δy .

Another interesting correlation is the distribution of the azimuthal angle ϕ . Pre-

liminary results for the azimuthal correlations in the k_T -factorization approach were considered in [23]. The main difference in the information coming from $d\sigma/dp_{pair}$ and $d\sigma/d\phi$ distributions is due to the comparatively slow heavy quark. It gives a negligibly small contribution to the $d\sigma/dp_{pair}$ in the first case, whereas in the second one each quark contributes to the distribution $d\sigma/d\phi$ practically independently of its momentum, so all corrections coming from quark confinement, hadronization and resonance decay can be important.

As was discussed above, the first contribution in Eq. (35) is the same as the conventional LO parton model in which the angle between the produced heavy quarks is always 180° . However the angle between two heavy hadrons can be slightly different from this value due to hadronization processes. To take this into account we assume that in this first contribution the probability to find a hadron pair with azimuthal angle $\phi = 180^\circ - \phi_1$ is determined by the expression

$$w_1(\phi_1) = \frac{p_h}{\sqrt{p_h^2 + p_T^2}}, \quad (36)$$

where $p_h = 0.2 \text{ GeV}/c$ is a transverse momentum in the azimuthal plane coming from the hadronization process. The other contributions of Eq. (35) result in a more or less broad ϕ distribution so we neglect their small modification due to hadronization.

The k_T -factorization approach predictions for the azimuthal correlation of heavy quarks produced in pp collisions are presented in Fig. 17. One can see that they change drastically when the initial energy increases from fixed target to the collider region.

There exists a lot of various correlations which have never been considered both theoretically and experimentally. Let us discuss several of them. In Fig. 18 we present the distribution on heavy quark pair transverse momentum in events, when the transverse momentum of one quark is fixed in the interval $p_{1T} = 19\text{--}21 \text{ GeV}/c$. These distributions are very sensitive to the scale value μ^2 in Eqs. (14), (17). In the case of $\mu^2 = \hat{s}$ both the charm and beauty distributions are practically flat for $p_{pair} < p_{1T}$ (with evident exception for the kinematical minimum at very small p_{pair}) and decrease rather fast for $p_{pair} > p_{1T}$. Such a behaviour again shows that the high transverse momentum of one heavy quark can be compensated by the second quark (region of comparatively small p_{pair} as well as by the hard gluon (region of $p_{pair} \sim p_{1T}$). For the smaller scale $\hat{s}/4$ in Eqs. (14), (17) the emission of hard gluons is suppressed and the dashed curves decrease immediately after the kinematical minima. Thus we can conclude that the measurement of this distribution allows to find the most reasonable scale value.

The scale problem can be solved if we will consider some distributions in different azimuthal angle regions. For example, the one-dimensional transverse momentum distribution is insensitive to the scale for back-to-back production ($\Delta\phi = 120^\circ - 180^\circ$) and rather sensitive for the smaller azimuthal angles, see Figs. 19 and 20.

The distribution over Δy at LHC energy is predicted to have minimum at the small azimuthal angles and Δy values in the case of comparatively small scale $\mu^2 = \hat{s}/4$ and to be more flat for the larger scale, see Figs. 21, 22.

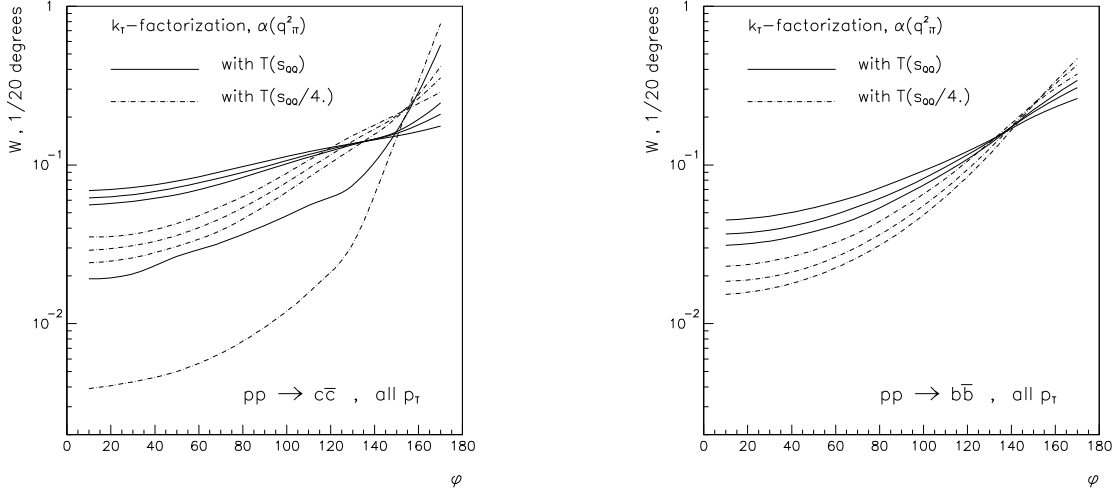


Fig. 17. The calculated azimuthal correlations of charm (a) and beauty (b) pair production for $\mu^2 = \hat{s}$ (solid curves) and $\mu^2 = \hat{s}/4$ (dash-dotted curves) at the energies equal to $\sqrt{s} = 14$ TeV (upper curves at small ϕ), 1.8 TeV, 630 GeV and 39 GeV (the latter one only for charm production).

7 Conclusion

We have compared the conventional LO Parton Model (PM) and the k_T -factorization approach for heavy quark hadroproduction at fixed target and collider energies using both "toy" and realistic gluon distributions. Both the transverse momenta and rapidity distributions have been considered, as well as several types of two-particle correlations, such as the distribution of the rapidity gap between two heavy quarks, their azimuthal correlations and distributions of the total transverse momentum of the produced heavy quark pair, p_{pair} .

It has been shown in Sect. 4 [28] that the contribution of the domain with strong q_T ordering ($q_{1T}, q_{2T} \ll m_T = \sqrt{m_Q^2 + p_T^2}$) coincides in the k_T -factorization approach with the LO PM prediction. Besides this a numerically large contribution appears at high energies in k_T -factorization approach in the region $q_{1,2T} \geq m_T$. This kinematically relates to the events where the transverse momentum of heavy quark Q is balanced not by the momentum of antiquark \bar{Q} but by the momentum of the nearest gluon.

This configuration is associated with the NLO (or even NNLO, if both $q_{1T}, q_{2T} \geq m_T$) corrections in terms of the PM with fixed number of flavours, i.e. without the heavy quarks in the evolution. Indeed, as was mentioned in [1], up to 80% of the whole NLO cross section originates from the events where the heavy quark transverse momentum is balanced by the nearest gluon jet. Thus the large "NLO" contribution, especially at large p_T , is explained by the fact that the virtuality of the t -channel (or u -channel)

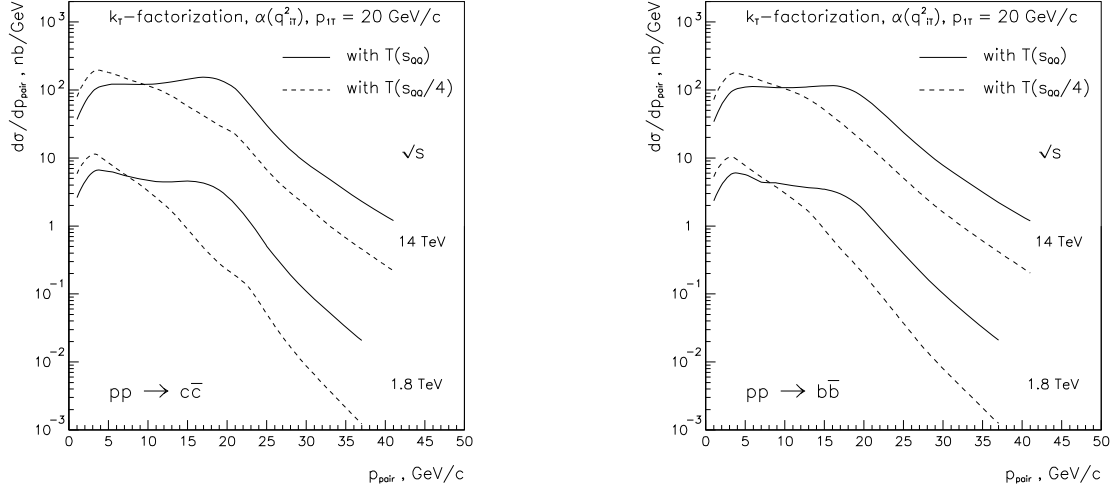


Fig. 18. The distributions of the total transverse momentum p_{pair} for c -quarks (a) and b -quarks (b) produced at different energies (solid curves) and with the transverse momentum of a one heavy quark restricted to the interval 19-21 GeV/c, calculated with the unintegrated gluon distribution $f_g(x, q_T, \mu)$ given by Eq. (14) and (17), for μ^2 values in Eq. (14) equal to \hat{s} . Dashed curves show the same distributions with scale $\mu^2 = \hat{s}/4$.

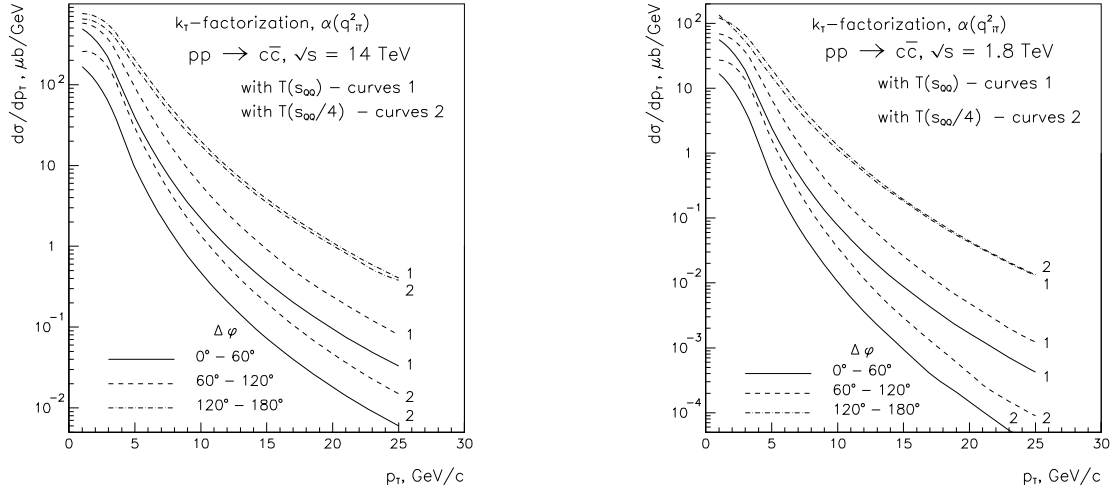


Fig. 19. p_T -distributions of c -quarks in different azimuthal angles produced at different energies.

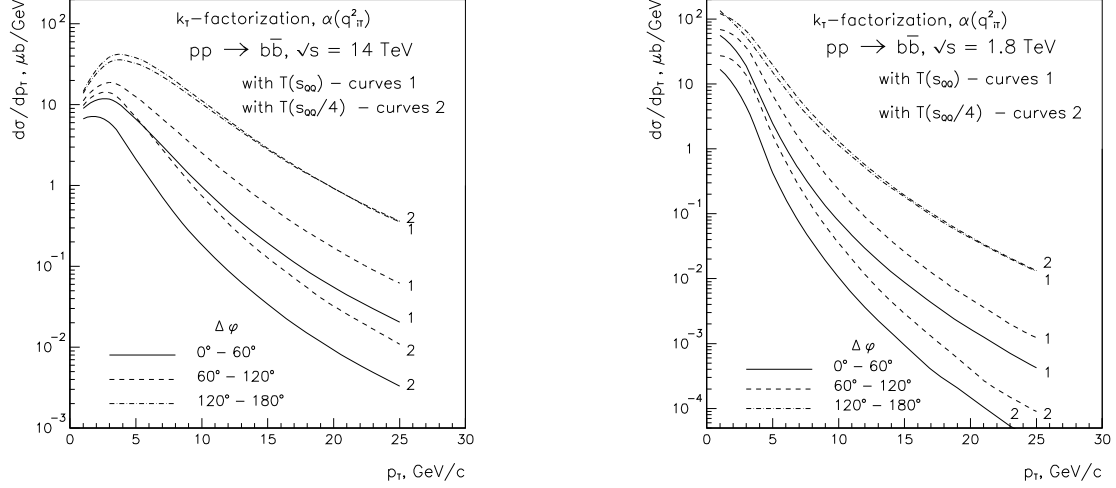


Fig. 20. p_T -distributions of b -quarks in different azimuthal angles produced at different energies.

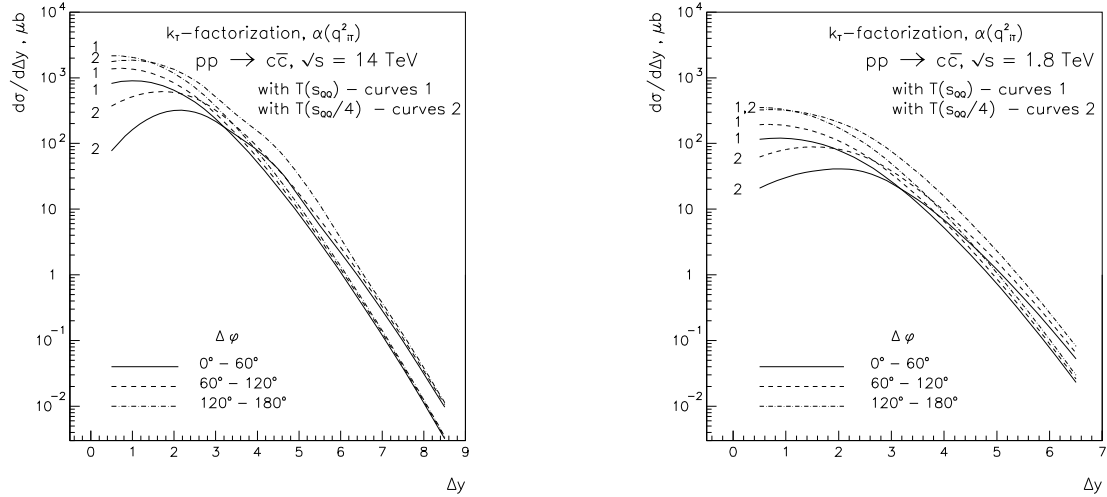


Fig. 21. The calculated distributions of the rapidity difference between two c -quarks produced at different azimuthal angles in the k_T factorisation approach.

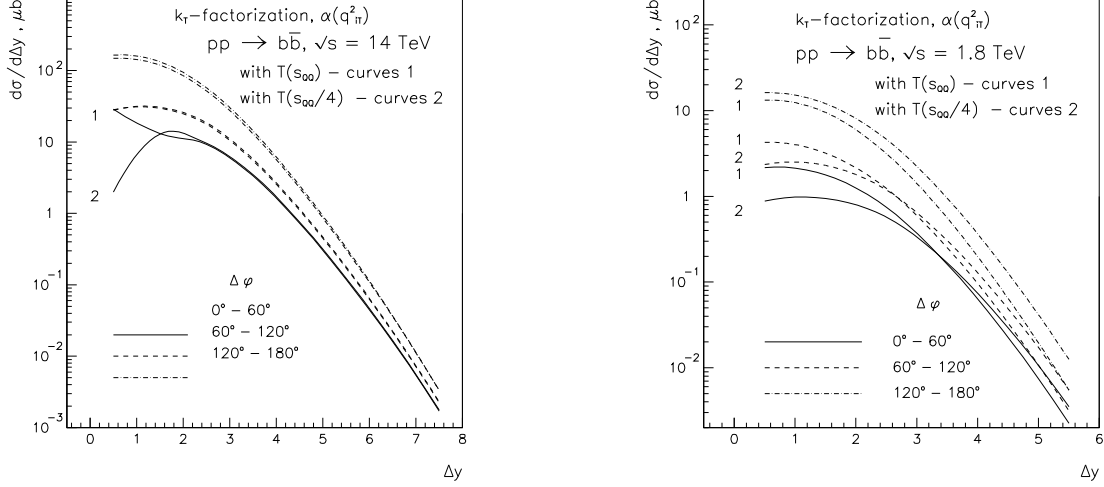


Fig. 22. The calculated distributions of the rapidity difference between two b -quarks produced at different azimuthal angles in the k_T factorisation approach.

quark becomes small in the region $q_T \simeq p_T$, and the singularity of the quark propagator $1/(\hat{p} - \hat{q} - m_Q)$ in the "hard" QCD matrix element, $M(q_{1T}, q_{2T}, p_{1T}, p_{2T})$, reveals itself.

The double logarithmic Sudakov-type form factor T in the definition of the unintegrated parton density Eq (17) comprises an important part of the virtual loop NLO (with respect to the PM) corrections. Thus we demonstrate that the k_T -factorization approach collects already at the LO the major part of the contributions which play the role of the NLO (and even NNLO) corrections to the conventional PM. Therefore we hope that a higher order (in α_S) correction to the k_T -factorization could be rather small.

Another advantage of this approach is that a non-zero transverse momentum of $Q\bar{Q}$ -system ($p_{Tpair} = p_{1T} + p_{2T} = q_{1T} + q_{2T}$) is naturally achieved in the k_T -factorization. We have calculated the p_{Tpair} distribution and compared it with the single quark p_T spectrum. At the low energies the typical values of p_{Tpair} are much lesser than the heavy quark p_T in accordance with collinear approximation. However for LHC energy both spectra become close to each other indicating that the transverse momentum of second heavy quark is relatively small. The typical value of this momentum ($p_{Tpair} = k_T$ -kick) depends on the parton structure functions/densities. It increases with the initial energy (k_T -kick increases with the decreasing of the momentum fractions x, y carried by the incoming partons) and with the transverse momenta of the heavy quarks, p_T . Thus one gets a possibility to describe a non-trivial azimuthal correlation without introducing a large "phenomenological" intrinsic transverse momentum of the partons.

It is necessary to note that the typical parton transverse momenta q_{1T} and q_{2T} increase in our calculations with the growth of the detected b -quark momentum p_T^{min} . In the language of k_T -kick it means that the values of $\langle k_T^2 \rangle$ also increase.

At the time being we would not like to compare our calculations with experimental data¹¹. It is shown that in all cases when a realistic gluon distribution is used the difference between our approach and the conventional parton model is not large, so our results should be in agreement with the data up to, say, a factor 2 or 3. At the same time the disagreement of such an order seems to be senseless to discuss, because the unintegrated gluon distributions are not known with the needed accuracy (from the evolution equation and the experimental data). Instead of them we have used more or less reasonable approximation Eq. (17). Although it is qualitatively good it can lead to a numerical disagreement. In particular, the angular ordering [47, 48, 49] implies that the cut-off $\Delta = q_T/\mu$ in Eqs. (14), (17) should be replaced by $\Delta = q_T/(\mu + q_T)$. From the formal point of view the difference is beyond the DGLAP LO accuracy. However with the new $\Delta = q_T/(\mu + q_T)$ one gets the non-zero values of $f_a(x, q_T, \mu)$ even at the large $q_T > \mu$. This is especially important at the high energies where the essential values of x and z (in Eq. (17)) are very small. The contribution coming from $q_T > \mu$ region could enhance the flux of colliding gluons up to a few times, and by this way explain the FNAL-Tevatron puzzle. These new data on the cross section of $b\bar{b}$ (or high- p_T prompt photon) production are 2-3 times larger than the conventional NLO PM QCD predictions [7, 10, 46]. At the moment we have no realistic unintegrated parton distributions which fit the data with accounting for the contribution from $q_T > \mu$.

That is why the presented here results are treated mainly as the qualitatively ones, having the numerical accuracy on the level of factor 2-3.

Another important point is that almost all presented results concern the heavy quarks rather than the hadron production. Of course, the hadronization leads to several important effects, such as different yields (asymmetry) of D - and \bar{D} -mesons production in pp collisions, see qualitative discussion in [56], however their quantitative description needs additional phenomenological assumptions, see e.g. [57, 58, 59, 60] or description of PYTHIA Monte Carlo code.

Acknowledgements

We are grateful to E.M.Levin who participated at the early stage of this activity and to many our colleagues for useful discussions. The presented calculations were carried out in part in ICTP. One of us (Y.M.S) is grateful to Prof. S.Randjbar-Daemi for providing this possibility and to the staff for creating good working conditions. We are grateful to Yu.L.Dokshitzer, G.P.Korchemsky and M.N.Mangano for discussions. This work was supported by grants NATO OTR.LG 971390 and RFBR 98-02-17629.

References

- [1] P.Nason, S.Dawson and R.K.Ellis. Nucl.Phys. B303 (1988) 607.

¹¹An example of very successful comparison in the k_T -factorization approach can be found in [17] where some different assumptions were used.

- [2] G.Altarelli et al. Nucl.Phys. B308 (1988) 724.
- [3] P.Nason, S.Dawson and R.K.Ellis. Nucl.Phys. B327 (1989) 49.
- [4] W.Beenakker,H.Kuijf, W.L.Van Neerven and J.Smith. Phys.Rev. D40 (1989) 54.
- [5] W.Beenakker, W.L.Van Neerven, R.Meng, G.A.Schuler and J.Smith. Nucl.Phys. B351 (1991) 507.
- [6] S.Frixione, M.N.Mangano, P.Nason and G.Ridolfi. Preprint CERN-TH/97-16 (1997); hep-ph/9702287.
- [7] B.Abbott et al. hep-ph/9905024; Submitted to Phys.Rev.Lett.
- [8] M.N.Mangano, P.Nason and G.Ridolfi. Nucl. Phys. B373 (1992) 295.
- [9] Yu.M.Shabelski. Talk, given at HERA Monte Carlo Workshop, 27-30 April 1998, DESY, Hamburg; hep-ph/9904492.
- [10] L.Apanasevich et al. Phys.Rev. D59 (1999) 074007.
- [11] P.Nason et al. hep-ph/0003142.
- [12] S.Catani, M.Ciafaloni and F.Hautmann. Phys.Lett. B242 (1990) 97; Nucl.Phys. B366 (1991) 135.
- [13] J.C.Collins and R.K.Ellis. Nucl.Phys. B360 (1991) 3.
- [14] G.Marchesini and B.R.Webber. Nucl.Phys. B386 (1992) 215.
- [15] S.Catani and F.Hautmann. Phys.Lett. B315 (1993) 475; Nucl.Phys. B427 (1994) 475.
- [16] S.Camici and M.Ciafaloni. Nucl.Phys. B467 (1996) 25; Phys.Lett. B396 (1997) 406.
- [17] P.Hägler et al. Phys.Rev. D62 (2000) 71502.
- [18] L.V.Gribov, E.M.Levin and M.G.Ryskin. Phys.Rep. 100 (1983) 1.
- [19] E.M.Levin and M.G.Ryskin. Phys.Rep. 189 (1990) 267.
- [20] E.M.Levin, M.G.Ryskin, Yu.M.Shabelski and A.G.Shuvaev. Sov.J.Nucl.Phys. 53 (1991) 657.
- [21] E.M.Levin, M.G.Ryskin, Yu.M.Shabelski and A.G.Shuvaev. Sov.J.Nucl.Phys. 54 (1991) 867.
- [22] M.G.Ryskin, Yu.M.Shabelski and A.G.Shuvaev. Z.Phys. C69 (1996) 269.
- [23] Yu.M.Shabelski and A.G.Shuvaev. Eur.Phys.J. C6 (1999) 313.
- [24] S.P.Baranov and M.Smizanská. Phys.Rev. D62 (2000) 014012.

- [25] Ya.I.Azimov, Yu.M.Shabelski and O.P.Strogoval. Phys.Atom.Nucl. 57 (1994) 674.
- [26] E.M.Levin, M.G.Ryskin and Yu.M.Shabelski. Phys.Lett. B260 (1991) 429.
- [27] Yu.M.Shabelski and D.Treleani. Phys.Lett. B403 (1997) 364.
- [28] M.G.Ryskin, Yu.M.Shabelski and A.G.Shuvaev. hep-ph/9907507.
- [29] M.G.Ryskin, Yu.M.Shabelski and A.G.Shuvaev. hep-ph/0007238.
- [30] M.Gluck, E.Reya and A.Vogt. Z.Phys. C67 (1995) 433.
- [31] M.Gluck, E.Reya and A.Vogt. Eur.Phys.J C5 (1998) 461.
- [32] J.C.Collins, D.E.Soper and G.Sterman. Nucl.Phys. B308 (1988) 833.
- [33] S.Narison. Phys.Lett. B341 (1994) 73; hep-ph/9503234.
- [34] P.Ball, M.Beneke and V.M.Braun. Phys.Rev. D52 (1995) 3929.
- [35] P.Nason, S.Dawson and R.K.Ellis. Nucl.Phys. B327 (1989) 49.
- [36] I.Sarcevic, P.Carruthers and Q.Gao. Phys.Rev. D40 (1989) 3600.
- [37] Liu Wenjie, O.P.Strogoval, L.Cifarelli and Yu.M.Shabelski. Yad.Fiz. 57 (1994) 900.
- [38] M.I.Adamovich et al. WA92 Coll. Nucl. Phys. B495 (1997) 3.
- [39] G.A.Alves et al. E769 Coll. Phys.Rev.Lett. 77 (1996) 2392.
- [40] BEATRICE Coll., M.Adamovich et al. Phys. Lett. B348 (1995) 256.
- [41] BEATRICE Coll., Y.Alexandrov et al. Phys. Lett. B433 (1998) 217.
- [42] C.Peterson, D.Schlatter, I.Schmitt and P.Zerwas. Phys.Rev. D27 (1983) 105.
- [43] J.Blümlein. Preprint DESY 95-121 (1995).
- [44] E.A.Kuraev, L.N.Lipatov and V.S.Fadin. Sov.Phys.JETP 45 (1977) 199.
- [45] G.Marchesini and B.R.Webber. Nucl.Phys. B310 (1988) 461.
- [46] M.A.Kimber, A.D.Martin and M.G.Ryskin. Eur.Phys.J. C12 (2000) 655; hep-ph/9911379.
- [47] M.Ciafaloni. Nucl.Phys. B296 (1988) 49.
- [48] S.Catani, F.Fiorane and M.Ciafaloni. Phys.Lett. B234 (1990) 339; Nucl.Phys. B336 (1990) 18.
- [49] G.Marchesini. In Proc. of the Workshop "QCD at 200 TeV", Erice, Italy (1990), ed. by L.Cifarelli and Yu.L.Dokshitzer, Plenum Press, New-York 1992, p.183.

- [50] Yu.L.Dokshitzer, D.I.Dyakonov and S.I.Troyan. Phys.Rep. 58 (1980) 270.
- [51] S.J.Brodsky, G.P.Lepage and P.B.Mackenzie. Phys.Rev. D28 (1983) 228.
- [52] G.P.Lepage. J.Comp.Phys. 27 (1978) 192.
- [53] J.Kwiechinski. Z.Phys. C29 (1985) 561.
- [54] M.N.Mangano, P.Nason and G.Ridolfi. Nucl. Phys. B405 (1993) 507.
- [55] Liu Wenjie, O.P.Strogova, L.Cifarelli and Yu.M.Shabelski. Phys.Atom.Nucl. 57 (1994) 844.
- [56] Yu.M.Shabelski. hep-ph/0011032.
- [57] A.K.Likhoded and S.R.Slabospitsky. Phys.Atom.Nucl. 60 (1997) 981; 62 (1999) 693; hep-ph/0008230.
- [58] T.Tashiro et al. hep-ph/9810284.
- [59] A.V.Berezhnoy, V.V.Kiselev and A.K.Likhoded. hep-ph-9905555.
- [60] J.Dias de Deus and F.Durães. Eur.Phys.J. C13 (2000) 647.